

A persistent behavioral state enables sustained predation of humans by mosquitoes

Trevor R. Sorrells^{1,2*}, Anjali Pandey¹, Adriana Rosas-Villegas¹, and Leslie B. Vosshall^{1-3*}

¹Laboratory of Neurogenetics and Behavior, The Rockefeller University, New York, NY 10065 USA, ²Kavli Neural Systems Institute, New York, NY 10065 USA, ³Howard Hughes Medical Institute, New York, NY 10065 USA. Current Address: Department of Biology, Brandeis University, 415 South Street, Waltham, MA 02453 United States (A.P.). For correspondence: trevorsorrells@gmail.com, leslie.vosshall@rockefeller.edu

Abstract Predatory animals pursue prey in a noisy sensory landscape, deciding when to continue or abandon their chase. The mosquito *Aedes aegypti* is a micropredator that first detects humans at a distance through sensory cues such as carbon dioxide. As a mosquito nears its target it senses more proximal cues such as body heat that guides it to a meal of blood. How long the search for blood continues after initial detection of a human is not known. Here we show that a 5-second optogenetic pulse of fictive carbon dioxide induced a persistent behavioral state in female mosquitoes that lasted for more than 10 minutes. This state is highly specific to females searching for a blood meal and was not induced in recently blood-fed females or in males, who do not feed on blood. In males that lack the gene *fruitless*, which controls persistent social behaviors in other insects, fictive carbon dioxide induced a long-lasting behavior response resembling the predatory state of females. Finally, we show that the persistent state triggered by detection of fictive carbon dioxide enabled females to engorge on a blood meal mimic offered up to 14 minutes after the initial 5-second stimulus. Our results demonstrate that a persistent internal state allows female mosquitoes to integrate multiple human sensory cues over long timescales, an ability that is key to their success as an apex micropredator of humans.

Introduction

Predatory animals first detect, then pursue, and ultimately capture prey (**Endler, 1991**). Because the pursuit phase can last for extended periods of time, it is critical for predators to persist in the chase even when the prey is not constantly detected. It is equally important for predators to abandon pursuit if enough time has elapsed that prey capture is unlikely to occur. This decision balances the need to obtain food with the expenditure of energy on unsuccessful hunts (**Anholt et al., 1987, Williams et al., 2014**). The duration of a pursuit could depend on the predator repeatedly sensing prey stimuli. Alternatively, it may be sustained by recent prior experience or a change in the internal state of the predator that outlasts individual prey stimuli.

Micropredators such as the mosquito consume small quantities of their live prey rather than killing them outright (**Lafferty et al., 2002**), but employ similar tactics to other pursuit predators. Female mosquitoes combine rich multisensory information from olfactory, visual,

44 taste, mechanosensory, and contact chemosensory systems to hunt humans from whom they
45 obtain blood to produce eggs. Carbon dioxide (CO₂) produced by human breath is highly
46 volatile, traveling long distances from the human host. Detection of CO₂ by the mosquito
47 results in an increase in flying behavior (**Eiras et al., 1991, McMeniman et al., 2014**) and
48 upwind flight (**Dekker et al., 2011, Dekker et al., 2005, Geier et al., 1999**) that is often
49 referred to as “activation”. However, mosquitoes require an additional, more proximal host cue
50 such as body heat or skin odor for short-range attraction and to engorge on blood (**Corfas et**
51 **al., 2015, Dekker et al., 2011, Dekker et al., 2005, Geier et al., 1999, McMeniman et al.,**
52 **2014, van Breugel et al., 2015**) (**Figure 1A**). In natural settings, human sensory cues are
53 typically brief and intermittent by the time they reach the mosquito due to turbulent air flows
54 and long distances (**Koehl, 2006**). However, studies of insect navigation have documented
55 only short-term responses to these stimuli on the order of a few seconds (**Álvarez-Salvado et**
56 **al., 2018, Dekker et al., 2011, Demir et al., 2020, Pang et al., 2018**). If mosquitoes possess
57 the ability to retain information about their prey and combine it with future information this may
58 explain their success at locating and feeding on human blood. Although the short-term role of
59 CO₂ in mosquito behavior has been known for nearly 100 years (**Rudolfs, 1922**), the idea that
60 CO₂ induces a long-term change in the internal state of the mosquito has not previously been
61 tested experimentally.

62
63 To study pursuit predation in the mosquito, we developed optogenetic tools to precisely deliver
64 short pulses of fictive CO₂. This allowed us to test the effect of activating CO₂ sensory neurons
65 with greater temporal resolution and without the continuous stimulus of air flow required for
66 delivery of real CO₂. We observed that detection of fictive prey led to a long-lasting behavioral
67 change in female mosquitoes. Following a 5-second fictive CO₂ stimulus, animals exhibited
68 high-arousal behaviors and engorged on a blood meal mimic offered up to 14 minutes later.
69 Neither males nor previously blood-fed females showed these effects, and this persistent
70 internal state was not induced by optogenetic stimulation of a sweet taste pathway.
71 Remarkably, males lacking the *fruitless* gene showed long-lasting responses to fictive CO₂
72 resembling those in females, consistent with our prior observation that these mutants show
73 some aspects of female mosquito behavior (**Basrur et al., 2020**). Our work identifies a
74 persistent internal state that may explain how mosquitoes aggressively pursue human hosts
75 for many minutes.

76

77 Results

78 Fictive CO₂ triggers blood feeding

79 We created optogenetic tools in *Aedes aegypti* mosquitoes that allowed us to precisely
80 activate sensory neurons that are specialized to detect CO₂. To do this we generated a
81 transgenic strain that expresses the red light-activated cation channel CsChrimson
82 translationally fused to the tdTomato fluorescent reporter (**Klapoetke et al., 2014**) under
83 control of the *QF2/QUAS* bipartite transcription system (**Potter et al., 2010**). We crossed this
84 transgene into a strain that expresses the QF2 transcription factor in neurons that express the
85 Gr3 CO₂ receptor subunit (**McMeniman et al., 2014, Younger et al., 2020**) (**Figure 1B**).
86 CsChrimson-tdTomato was detected in maxillary palp neurons but not antennal neurons,
87 consistent with the observation that maxillary palp neurons are exquisitely sensitive to CO₂
88 (**Grant et al., 1995**) (**Figure 1C,D**). As expected, we found that CsChrimson-expressing
89 neurons extended axons that innervated glomerulus MD1 in the antennal lobe of the mosquito

90 brain (Figure 1E), which is known to be CO₂-sensitive (Younger et al., 2020). To test whether
91 mosquitoes responded to optogenetic activation of CO₂ sensory neurons, we presented
92 animals with a 5-second red light (627 nm) stimulus and tracked their movement (Figure 1F-I).
93 Control animals carrying only the *Gr3-QF2* driver or the *QUAS-CsChrimson* transgene reporter
94 showed no response to red light. However, mosquitoes with both genetic elements (*Gr3 >*
95 *CsChrimson*) increased their velocity in response to the stimulus (Figure 1H-I). This is
96 consistent with the known role of CO₂ in activating mosquitoes.

97
98 When combined with another host cue such as heat, CO₂ is sufficient to elicit blood feeding in
99 female mosquitoes (McMeniman et al., 2014). To test whether fictive CO₂ sensation triggered
100 by optogenetic activation of *Gr3* sensory neurons could replace real CO₂, we created a
101 behavior assay called the opto-membrane feeder (Figure 1J). This assay consists of a
102 cylindrical canister of mosquitoes surrounded by red light-emitting diodes (LEDs) and a warm
103 blood meal behind a membrane sitting on top of the mesh lid. Mosquitoes were presented with
104 either CO₂, fictive CO₂ via red light, or neither stimulus. Control mosquitoes with either *Gr3-*
105 *QF2* or *QUAS-CsChrimson* were attracted to the warm blood meal and engorged only when
106 presented with CO₂ but not when presented with red light (Figure 1K-M). In contrast, *Gr3 >*
107 *CsChrimson* mosquitoes were attracted and engorged in the presence of either real or fictive
108 CO₂, the latter delivered as a red-light stimulus (Figure 1K-M). These results demonstrate that
109 mosquitoes interpreted optogenetic activation of the CO₂ sensory neurons as a host cue that is
110 sufficient to drive blood feeding.

112 Fictive CO₂ induces prolonged host-seeking behaviors

113 Host-seeking begins when female mosquitoes detect a human, typically by sensing volatile
114 cues like CO₂. Once activated by human odorants, they seek out the source of the cues, and
115 upon landing, mosquitoes walk to locate a patch of skin to pierce. To understand the timing
116 and nature of the mosquito response to transient host cues, we created an assay called the
117 opto-thermocycler (Figure 2A-B). In this assay mosquitoes receive optogenetic light stimulation
118 from above and heat through the mesh at the bottom of the assay chamber. The use of fictive
119 CO₂ delivered optogenetically was critical for studying the internal state of the mosquito after
120 these transient host cues. Delivery and removal of real CO₂ necessitates constant air flow,
121 which is itself an important sensory cue for insects.

122
123 We employed machine-learning based behavior classification as a high-throughput readout of
124 mosquito behavioral responses (Figure 2C-D). We tracked nine points on the mosquito body
125 using Animal Part Tracker and four behaviors using JAABA (Kabra et al., 2013): grooming,
126 flying, walking, and probing, a behavior in which the mosquito inserts its proboscis through the
127 mesh in the bottom of the container. When none of these four behaviors were present,
128 mosquitoes were predominantly motionless, showed slow hindleg movement, or occasionally
129 flailed against the wall of the assay chamber without walking. All classifiers showed high
130 accuracy with >90% true positive and true negative rates on a set of test video frames
131 (Supplementary File 1).

132
133 We delivered 5-second red light pulses and heat increases to simulate brief CO₂ and human
134 body heat stimuli (Figure 2B). Mosquitoes responded to individual heat and fictive CO₂ stimuli
135 with elevated walking, flying, and probing (Figure 2E-H, Figure 2—figure supplement 1). The

136 response to heat alone was dominated by probing and returned to baseline after about one
137 minute ($t_{1/2 \text{ probing}} = 0.4$ minutes). In contrast, fictive CO₂ alone caused an immediate flight and
138 probing response followed by sustained walking, flying, and probing (Figure 2H, Figure 2—
139 figure supplement 1, Supplementary Video 1) that took approximately 15 minutes to return to
140 baseline ($t_{1/2 \text{ probing}} = 3.9$ minutes). The long duration of the response to CO₂ is reminiscent of
141 persistent internal states in other organisms (Asahina et al., 2014, Flavell et al., 2013,
142 Hindmarsh Sten et al., 2021, Marques et al., 2020).

143
144 These observations of mosquito behavior could reflect an internal state specific to host-
145 seeking behavior or a general arousal state elicited by many sensory stimuli. Like CO₂, bright
146 light is also an arousal signal in mosquitoes (Araripe et al., 2018) so we asked whether bright
147 light induces a long-lasting behavior state. Mosquitoes have weaker visual sensitivity to red
148 wavelengths (San Alberto et al., 2021), and we saw no behavioral response to red light
149 (Figure 2E), so we used green light. Because this experiment is designed to test whether
150 mosquitoes have a response to a visual stimulus, a question that does not depend on the use
151 of optogenetics, we used wild-type mosquitoes. A bright green light stimulus induced a brief
152 response dominated by walking ($t_{1/2 \text{ walking}} = 0.4$ minutes), much shorter than the response to
153 fictive CO₂ (Figure 2I,K).

154
155 While CO₂ and heat elicit the blood-feeding program required for females to produce eggs,
156 mosquitoes possess a second, distinct feeding program for ingestion of flower nectar for
157 energy (Jové et al., 2020, Lahondere et al., 2020). We asked whether optogenetic stimulation
158 of *Gr4* sensory neurons that are thought to detect sugar evoked a sustained behavior
159 response in mosquitoes as with optogenetic activation of the CO₂ sensory neurons. We found
160 that fictive sugar elicited a response composed largely of probing that was of shorter duration
161 than fictive CO₂ ($t_{1/2 \text{ probing}} = 1.5$ minutes) (Figure 2J,L).

162
163 The temporal resolution of our assays allowed us to understand precisely how mosquitoes
164 integrate CO₂ and heat to affect their behavior. We focused on the first 15 seconds after
165 stimulus onset during which the greatest behavior responses are seen. We found that the
166 heightened probing response seen when the stimuli were presented together was roughly
167 additive with respect to the individual stimuli (Figure 2M, Figure 2—figure supplement 2). In
168 contrast, flying was strongly suppressed. This demonstrates that multimodal integration of host
169 cues biases action selection away from long-range flight and toward a short-range probing
170 behavior.

171
172 Heat is a host cue but also may be experienced by the mosquito under other environmental
173 contexts. We compared the integration of heat with green light and fictive sugar to see if they
174 are integrated similarly to the host cue CO₂. In contrast to the integration of host cues, probing
175 was suppressed when non-host cues were presented together (Figure 2M, Figure 2—figure
176 supplement 2). This demonstrates that the mosquito nervous system uses different
177 computations for the integration of host cues and non-host cues.

178 179 **The CO₂-evoked persistent state is specific to host seeking**

180 The fact that bright green light and fictive sugar stimuli elicited briefer responses suggested
181 that the prolonged response to fictive CO₂ is specific to host seeking. If true, it should be

182 modulated similarly to host-seeking behavior. Host seeking in *Aedes aegypti* is suppressed
183 after a female takes a blood meal, only returning after she lays eggs several days later (**Duvall**
184 **et al., 2017, Klowden, 1981**). We allowed female mosquitoes to blood feed on a human arm
185 and then assayed their behavior four days later (**Figure 3A,B,D,E**). We found that blood-fed
186 females completely lost their response to fictive CO₂ and nearly completely lost their response
187 to heat. This demonstrates that in addition to losing the persistent state, blood-fed females lose
188 even brief responses to host cues.

189
190 Unlike females, male mosquitoes do not seek out hosts to feed on blood. Males do
191 demonstrate a flight response to CO₂ (**Matthews et al., 2016**) and are reported to congregate
192 in the vicinity of humans where they mate with female mosquitoes (**Hartberg, 1971**). We
193 observed that male mosquitoes had minimal responses to heat, but substantial flight and
194 walking responses to fictive CO₂ (**Figure 3C-E**). However, the response to fictive CO₂ was
195 brief, decaying rapidly back to baseline ($t_{1/2 \text{ probing}} = 0.4$ minutes). This observation suggests
196 that the persistence—but not the initial response—is specifically regulated in a sexually
197 dimorphic manner.

198
199 We have previously shown that *fruitless* mutant male mosquitoes gain strong attraction to
200 human odor (**Basrur et al., 2020**). We asked whether these *fruitless* mutant males have an
201 altered response to fictive CO₂ stimuli. First, we confirmed that *fruitless* mutant males lacking
202 *Gr3 > CsChrimson* did not respond to red light, as expected (**Figure 3F**). *fruitless*
203 heterozygotes receiving fictive CO₂ showed a brief response ($t_{1/2 \text{ probing}} = 0.4$ minutes) (**Figure**
204 **3G,I,J**), similar to the response we saw for wild type males (**Figure 3C**). By comparison,
205 *fruitless* mutant males receiving fictive CO₂ showed a strong and sustained response for
206 minutes after the stimulus ($t_{1/2 \text{ probing}} = 1.7$ minutes) (**Figure 3H-J**). Thus, *fruitless* regulates the
207 persistent host-seeking state by suppressing this behavior in males. We note that the duration
208 of the sustained response of *fruitless* mutant males is shorter than in females, suggesting
209 additional sexually dimorphic factors may regulate this internal state. Taken together, these
210 results demonstrate that blood-fed females and males, which do not engage in blood-feeding
211 behavior, lack sustained responses to brief pulses of fictive CO₂. Males lacking the gene
212 *fruitless* were previously reported to show strong attraction to human scent (**Basrur et al.,**
213 **2020**) and we show here that they also demonstrate strong and long-lasting responses to
214 fictive CO₂ reminiscent of females. This raises the possibility that the persistent state is the
215 behavioral mechanism by which the goal of blood feeding is sustained in the female mosquito.

216 217 **Mosquitoes integrate sensory cues for minutes**

218 Motivation consists of two components: increased arousal and directed action toward a goal.
219 We have demonstrated that fictive CO₂ induces a prolonged increase in movement and the
220 probing behavior that immediately precedes blood feeding. We asked whether the persistent
221 state induced by a brief pulse of fictive CO₂ can influence the response to body heat and
222 ultimately if it can induce blood feeding many minutes afterwards.

223
224 First, we tested whether fictive CO₂ primes subsequent responses to heat (**Figure 4A**).
225 Because CO₂ is highly volatile, mosquitoes likely sense this cue before body heat in
226 naturalistic host-seeking settings. When we presented heat first followed by fictive CO₂,
227 relatively small behavioral responses were evoked (**Figure 4B-C**). However, when fictive CO₂

228 was presented simultaneously with heat or 15 or 60 seconds prior to heat, larger walking and
229 probing responses were seen (Figure 4B-C). This suggests that mosquitoes respond most
230 strongly to the naturalistic temporal order of these host cues. Next, we asked how long prior to
231 the heat stimulus fictive CO₂ can boost the response (Figure 4D). Compared to heat alone,
232 walking and probing were increased when a fictive CO₂ stimulus was presented up to four
233 minutes prior (Figure 4E-F). This demonstrates that in addition to the sustained behavior
234 response, fictive CO₂ increases the response to heat for minutes afterward.

235
236 Once a mosquito pierces the skin of a human host, taste cues present in the blood guide the
237 decision to engorge. Because this is the final goal of host-seeking behavior, we wondered
238 whether mosquitoes in the fictive CO₂-triggered persistent state had altered responses to both
239 heat and taste stimuli. To test this, we designed an opto-feeder assay that incorporated a thin
240 sheet of a blood meal mimic located between the thermocycler heating element and the mesh
241 below the mosquito, allowing it to be rapidly heated and cooled (Figure 4G-H). We used a
242 solution of ATP in saline, which has previously been shown to be a highly palatable meal that
243 induces females to engorge in the same manner as blood (Galun et al., 1963, Jové et al.,
244 2020). This allowed us to test how the prolonged arousal state induced by fictive CO₂
245 influences the decision of the mosquito to feed on a blood meal mimic.

246
247 First, we explored the temporal relationship of host stimuli to test whether the naturalistic order
248 of CO₂, heat, and taste stimuli elicits greater rates of feeding. When fictive CO₂ was presented
249 along with heating of the meal for 10 minutes, many females fed to repletion (Figure 4I). To
250 test the temporal order of these cues, we offered fictive CO₂ and a meal that was only warmed
251 for several minutes, resulting in reduced feeding levels (Figure 4I). When the order was
252 swapped and females were briefly offered the warm meal prior to fictive CO₂, very few females
253 fed (Figure 4I). This suggests that mosquitoes feed at the highest rates when they receive a
254 CO₂ stimulus prior to heat and taste stimuli. Next, we asked how long after a brief pulse of
255 fictive CO₂ females would retain the motivation to feed on the blood meal mimic. When offered
256 the warm meal without fictive CO₂, few females fed. We then stimulated the females with fictive
257 CO₂ and heated the blood meal mimic either immediately or after a delay of 2, 8, 14, or 20
258 minutes after fictive CO₂. We hypothesized that if the fictive CO₂ induced a persistent state of
259 host seeking, it might trigger engorging behavior many minutes later. Indeed, fictive CO₂ was
260 able to potentiate feeding when presented up to 14 minutes prior to heating of the blood meal
261 mimic (Figure 4J). Taken together, our results demonstrate that the persistent host-seeking
262 state increases host-seeking behaviors and alters the response to sensory cues for many
263 minutes after a brief fictive CO₂ stimulus. We speculate that this reflects the amount of time a
264 mosquito will pursue a host in a naturalistic setting before halting the search if it appears that
265 the host is no longer nearby.

266
267 We noticed that there is considerable individual variation in how mosquitoes respond to the
268 warm blood meal mimic after being activated by fictive CO₂ (Figure 4J). We asked whether the
269 behavior state of individual mosquitoes could be inferred over longer periods of time. We
270 extracted 38 behavior parameters from the experiment in Figure 4J from 30-second-long time
271 windows and used t-distributed stochastic neighbor embedding (tSNE) to visualize the
272 relationships. This embedding revealed that mosquito behavior fell into four major states that
273 we termed rest, global search, local search, and engorge (Figure 4K, Figure 4—figure

274 **supplement 1**). These states were observed even when the length of the time window was
275 varied over a 6-fold range (**Figure 4—figure supplement 2**). The states differed in the
276 proportions of behaviors observed, the transition rates between them, and the total distance
277 the mosquito travelled while in each state. We divided the data into those females that
278 eventually fed or did not feed at the end of the experiment (**Figure 4L**). As expected, the
279 engorge state was greatly enriched in mosquitoes that were categorized as fed, demonstrating
280 that this method is effective at identifying longer-timescale behavior states (**Figure 4L**).

281
282 We asked whether the behavior state of the mosquito after fictive CO₂ was associated with the
283 future decision to feed on the warm blood meal mimic. We found that fed and unfed
284 mosquitoes showed similar amounts of global search pre-heat but greater levels of local
285 search for those that would later feed (**Figure 4M**). The local search state differs primarily by
286 showing more probing and less flight than the global search state. To avoid potential
287 distortions created by the 2-dimensional embedding (**Chari et al., 2021**), we trained a linear
288 classifier using only the four behaviors (groom, walk, flight, and probe). A classifier trained on
289 the proportion of time mosquitoes spent in each behavior for 2 minutes after the light stimulus
290 could predict which mosquitoes would later feed with above-chance accuracy (**Figure 4N**).
291 Thus, the behavior state that individual mosquitoes enter in response to fictive CO₂ reflects the
292 likelihood of response to future sensory cues.

293

294 Discussion

295 We investigated how female mosquitoes pursue humans by combining multisensory stimuli in
296 time to achieve the goal of feeding on human blood. To precisely control the delivery of CO₂,
297 we generated optogenetic tools to deliver fictive CO₂ and combined this with high-resolution
298 behavior assays and machine learning analysis approaches. These experiments demonstrated
299 that optogenetic activation of CO₂ sensory neurons induced a long-lasting behavior state
300 change (**Figure 4O**). During this time mosquitoes had heightened responses to heat and were
301 more likely to feed on a blood meal mimic even if encountered minutes after the CO₂ stimulus.

302

303 Integration of sensory information over time allows the nervous system to optimize decision
304 making for a particular goal (**Körding, 2007**). Testing whether predators use this approach
305 during hunting requires a precise understanding of what the predator is sensing and when,
306 precluding field studies. Laboratory studies have found behavior responses altered for as long
307 as a few seconds after encountering CO₂ in mosquitoes and other olfactory stimuli in
308 *Drosophila* (**Álvarez-Salvado et al., 2018, Dekker et al., 2011, Demir et al., 2020, Pang et**
309 **al., 2018**). Although this timescale of sensory integration is sufficient for upwind tracking,
310 modelling suggests that integration over long timescales can maximize the information about
311 the location of an olfactory stimulus (**Vergassola et al., 2007**). Here, we show that mosquitoes
312 integrate olfactory, heat, and taste stimuli for at least 14 minutes, much longer than previously
313 assumed. The increased movement and the bias of actions toward a particular goal constitute
314 an internal motivational state sustained over minutes—one specific to feeding on humans.
315 Importantly, our results show that this internal state does not require constant flight behavior or
316 a constant air flow stimulus, demonstrating that it is maintained by an internal mechanism
317 rather than continuous sensory or reafferent stimuli.

318

319 In principle, the long-duration characteristic of the host-seeking state could be generated by
320 neurons at any point in the circuit. However, it is extensively documented in *Aedes aegypti* that
321 CO₂ sensory neurons show an accurate readout of CO₂ levels over a large concentration
322 range (**Grant et al., 2007, Grant et al., 1995**). These neurons do not show adaptation or
323 prolonged activity (**Grant et al., 1995**) and have similar responses in males and females
324 (**Grant et al., 2007**). While we suspect, based on precedents for persistent states observed in
325 other systems, that the persistent state is controlled in the central brain, we cannot exclude a
326 contribution from the periphery. In mice, circuits originating in the central amygdala promote
327 pursuit and attack during cricket hunting (**Han et al., 2017**), but these behaviors appear time-
328 locked to optogenetic activation and a circuit controlling hunting persistence has not been
329 identified.

330
331 Mosquito host seeking shares some characteristics with other social and feeding states
332 (**Asahina et al., 2014, Flavell et al., 2013, Hindmarsh Sten et al., 2021, Marques et al.,**
333 **2020**). The pursuit of females by males during courtship behavior in *Drosophila* shows
334 especially striking similarities. In response to female sensory cues or stimulation of a subset of
335 *fruitless* neurons, male flies enter a state of increased courtship behaviors and lower
336 thresholds for sensory cues from females (**Clowney et al., 2015, Hindmarsh Sten et al.,**
337 **2021, Inagaki et al., 2014, Jung et al., 2020**). It appears that this function of *fruitless* is
338 conserved and displays the properties of persistence and sexual dimorphism (**Bertossa et al.,**
339 **2009, Demir et al., 2005, Manoli et al., 2005**). These similarities suggest that mosquito
340 evolution may have co-opted these properties of ancestral *fruitless* circuits to drive a novel
341 feeding behavior.

342
343 This study illuminates why mosquitoes are such effective predators: they maintain the goal of
344 blood feeding for minutes even in the absence of any additional positive stimuli or
345 reinforcement. Because this state greatly outlasts individual sensory stimuli and integrates
346 multiple modalities, any intervention that disrupts this internal drive state should be more
347 effective than vector control measures that mask or disrupt any individual aspect of host-
348 seeking.

349

350 **Methods**

351 **Human and animal ethics statement**

352 Blood feeding of mosquitoes with live mice was conducted according to IACUC protocol
353 17108. Blood feeding of mosquitoes with human subjects was conducted according to IRB
354 protocol LV-0652. Human subjects gave written informed consent to participate in the
355 experiments.

356

357 **Mosquito strains**

358 The following *Aedes aegypti* strains were used in this paper: wild type Liverpool, *Gr3-QF2*
359 (**Younger et al., 2020**), *Gr4-QF2* (**Jové et al., 2020**), *fruitless*^{ΔM} (**Basrur et al., 2020**),
360 *fruitless*^{ΔM-tdTomato} (**Basrur et al., 2020**), and *QUAS-CsChrimson* (this study).

361

362 **Mosquito rearing**

363 Mosquito strains were reared at 26°C ± 2°C with 80% humidity and 14 hours light, 10 hours
364 dark (lights on at 7AM) as previously described (**DeGennaro et al., 2013**). Embryos were

365 hatched in hatching broth: 1 pellet of fish food (TetraMin Tropical Tablets, Pet Mountain
366 16110M) crushed using a mortar and pestle, added to 850 mL deionized water, then
367 autoclaved. Larvae were reared in deionized water and fed 1-3 tablets of fish food per day.
368 Adult mosquitoes were fed on 10% sucrose (w/v in distilled water) ad libitum. Sucrose was
369 delivered in a Boston clear round 60 mL glass bottle (Fisher FB02911944) filled with 50 mL
370 10% sucrose. A cotton dental wick (Richmond Dental 201205) was inserted into the bottle and
371 mosquitoes fed from the sugar-moistened wick. Female mosquitoes were blood fed on mice or
372 human arm to generate eggs. Eggs were dried at 26°C and 80% humidity for 3 days, and then
373 stored at ambient temperature and humidity for up to 3 months. Adults were allowed to mate
374 freely for at least 7 days prior to performing experiments. All behavior experiments were
375 carried out in the light phase of the photoperiod, with most experiments occurring between
376 Zeitgeber (ZT) ZT2 to ZT12.

377 378 **Creation of CsChrimson mosquitoes for optogenetics**

379 We generated mosquitoes that expressed a translational fusion of CsChrimson to tdTomato
380 under the control of the QUAS promoter, referred to as *CsChrimson* or *QUAS-CsChrimson*
381 throughout the paper. The coding sequence of *CsChrimson-tdTomato* was PCR-amplified from
382 the vector p20X (Klapoetke et al., 2014) using the following oligonucleotide primers: forward
383 5'-CTCGAGCAAATGAGCAGACTGGTCGCCGCTTC-3', reverse 5'-
384 ATCCTCTAGATTACACCTCGTTCTCGTAGCAGAATTTATACAG-3'. The vector backbone
385 from pXL-BacII (Riabinina et al., 2016) was amplified by PCR using the following
386 oligonucleotide primers: forward 5'-GTCTGCTCATTGCTCGAGCCGCGGCCGCAGATC-3',
387 reverse 5'-CGAGGTGTAATCTAGAGGATCTTTGTGAAGGAACCTTACTTCTG-3'. The insert
388 was cloned into the backbone using Infusion HD cloning kit (Takara 638920) to create pTS26,
389 available at Addgene (plasmid number 175548). This plasmid was injected into 500 *Aedes*
390 *aegypti* Liverpool embryos by the Insect Transformation Facility (Rockville, MD) using 200
391 ng/μL plasmid DNA and 200 ng/μL piggyBac transposase mRNA. Ten independent *QUAS-*
392 *CsChrimson* integration events were isolated under standard mosquito rearing conditions.

393 394 **Peripheral sensory appendage microscopy**

395 Mosquitoes 3-4 weeks of age were anesthetized on ice, then maxillary palps and antennae
396 were removed using sharp forceps and placed in fixative (4% paraformaldehyde, 0.1M
397 Millonig's Phosphate Buffer pH 7.4, 0.25% Triton X-100) and nutated for 30 minutes at 4°C.
398 Tissues were washed four times in PBS, then mounted in SlowFade Diamond Antifade
399 Mountant (ThermoFisher). Images were acquired on an Inverted LSM 780 laser scanning
400 confocal microscope (Zeiss) using a 25x 0.8 NA multi-immersion objective with oil. Images
401 were processed using ImageJ.

402 403 **Brain Immunostaining**

404 Brain immunostaining was carried out as previously described (Jové et al., 2020). Mosquitoes
405 1-2 weeks of age were anesthetized on ice, then heads were removed using forceps and
406 placed into fixative (4% paraformaldehyde, 0.1M Millonig's Phosphate Buffer pH 7.4, 0.25%
407 Triton X-100) and nutated for 3 hours at 4°C. Heads were washed four times in PBS and kept
408 on ice during dissections. The brains were dissected using #5 forceps (Dumont) in a droplet of
409 PBS on a Petri dish coated with SYLGARD silicone elastomer (Dow). Brains were transferred
410 to a 35 μm mesh cap of a flow cytometry test tube (Fisher 08-771-23) in a 24-well plate

411 containing PBSTx (PBS with 0.25% Triton X-100). Brains were washed four times for 30-60
412 minutes at room temperature in PBSTx on an orbital shaker before permeabilization and
413 between each of the following steps. Brains were permeabilized in PBS with 4% Triton X-100
414 and 2% normal goat serum for 2 days at 4°C on an orbital shaker. We used the mouse anti-
415 Bruchpilot (brp) monoclonal antibody at a dilution of 1:10,000. The brp antibody was purified by
416 Frances Weis-Garcia of the Sloan Kettering Institute Antibody & Bioresource from the brp/nc82
417 hybridoma, developed by Erich Buchner at the Universitätsklinikum Würzburg and obtained
418 from the Developmental Studies Hybridoma Bank, created by the NICHD of the NIH and
419 maintained at The University of Iowa, Department of Biology, Iowa City, IA 52242. Rabbit anti-
420 RFP antibody (Rockland 600-401-379) was used at a dilution of 1:1000 to detect tdTomato
421 fused to CsChrimson. Brains were incubated in primary antibodies in PBSTx with 2% normal
422 goat serum for 3 days at 4°C on an orbital shaker. Secondary antibodies were goat anti-mouse
423 Alexa Fluor 647 (Thermo Fisher A21235) and goat anti-rabbit Alexa Fluor 555 (Thermo Fisher
424 A32732) both at 1:500 dilution. Brains were incubated in secondary antibodies in PBSTx and
425 2% normal goat serum for 2 days at 4°C on an orbital shaker. Brains were washed four more
426 times at room temperature for 30-60 minutes before mounting in SlowFade Diamond Antifade
427 Mountant (ThermoFisher). Images were acquired on an Inverted LSM 880 Airyscan NLO laser
428 scanning confocal microscope (Zeiss) using a 25x 0.8 NA multi-immersion objective with oil.
429 Images were processed using ImageJ.

430

431

Rearing mosquitoes for optogenetics

432 For CsChrimson to respond to red light (625 nm in this paper), it is necessary to supply the all-
433 trans retinal co-factor. Moreover, it is critical that animals reared for optogenetics be
434 maintained in the dark to avoid activating CsChrimson inappropriately. Therefore, we
435 developed a mosquito rearing protocol to deliver all-trans retinal under dark conditions. First,
436 we carried out experiments to select the best *QUAS-CsChrimson* transgenic insertion among
437 the 10 lines we generated. We wanted lines with strong and selective behavioral induction in
438 combination with a QF2 driver, but no basal behavioral activity without a QF2 driver. We also
439 wanted it to be a single insertion at a known position in the genome, that would not obviously
440 disrupt a known gene. The insertion site of the transgene in each line was mapped to the
441 genome using TagMapping (**Stern, 2017**). After being fed with all-trans retinal as described
442 below, all 10 lines were tested for their response to red light with and without being crossed to
443 a QF2 driver. Based on these initial screens, a single line with the *QUAS-CsChrimson*
444 transgene inserted in an intron of the gene LOC23687794 on chromosome 2 at base pair
445 453,953,698 in the L5.0 version of the *Aedes aegypti* genome (**Matthews et al., 2018**) was
446 selected for use in all subsequent experiments. This *CsChrimson* strain was outcrossed to wild
447 type mosquitoes for 8 generations before being homozygosed and used for behavior
448 experiments. For all experiments except those in **Figure 2I,K**, which used wild type mosquitoes
449 with a green light startle stimulus, animals were subjected to special rearing conditions to
450 prepare them for optogenetics. Eggs were hatched in 1 L of hatching broth under a 14-hour
451 450 nm blue light and a 10-hour dark cycle in a light-tight 26°C incubator with 80% humidity.
452 Blue light was selected for the light phase of the photoperiod to avoid activating CsChrimson.
453 The next day 2 L of distilled water was added to the pan, and the following day larvae were
454 thinned to 450 per pan. Larvae were subsequently sorted for fluorescence markers if
455 necessary, using a dissecting microscope. Larvae were fed daily with 1-3 tablets of Tetramin
456 fish food (Pet Mountain 16110M) ground into a powder using a mortar and pestle. Pupae were

457 moved to eclose into adults in a 30 cm x 30 cm x 30 cm insect rearing cage (Bugdorm
458 DP1000) with ad libitum access to 10% sucrose in sugar-feeding glass bottles. Animals were
459 not sexed at this stage, so cages contained males and females that freely mated. Behavior
460 experiments were performed 1-4 weeks post-pupation. Three days before the experiment, the
461 sugar wicks were replaced with water wicks to starve animals for 24 hours. Two days before
462 the experiment, the water wicks were replaced with wicks soaked in 10% sucrose and 400 μ M
463 all-trans retinal (Sigma, R2500-1G). 50 mL of sucrose and all-trans retinal was used per cage.
464 Animals were allowed to feed for 1-3 days in the dark on this meal. In pilot experiments we
465 verified that starved females fed on sucrose and all-trans retinal by observing yellow
466 pigmentation in the abdomen. Feeding in the dark was used to avoid premature neuronal
467 activation and bleaching of the all-trans retinal in the sugar feeders. This rearing protocol was
468 used for all experiments in the opto-membrane feeder, opto-thermocycler, and opto-feeder
469 experiments.

470

471 **Opto-membrane feeder assay**

472 The optomembrane feeder assay was constructed using optomechanical components
473 (Thorlabs MB12, TR12, RA90) and a black 1/4" thick acrylic platform for the canister of
474 mosquitoes to rest on. A hole in the bottom of the platform allowed a camera (Blackfly U3-
475 13S2M-CS, FLIR) outfitted with an 800 nm longpass filter (Midwest Optical LP800-34) to
476 image through the clear canister. Canisters were constructed from a polycarbonate tube of
477 diameter 4.5" (McMaster-Carr 8585K56) and 5" long. The bottom was made of clear 1/8" thick
478 acrylic and attached with plastic epoxy (Loctite 1363118). The top was an inset lid made of
479 black 1/4" and 1/8" inch acrylic and UV-resistant black mesh (McMaster-Carr 87655K13). The
480 canister was surrounded by a coil of RGB LEDs (Digikey 289-1189-ND) spaced 1.5" from the
481 exterior of the canister and controlled by an Arduino Uno board (Arduino A000066).
482 Mosquitoes were illuminated by 850 nm infrared LEDs surrounding the top of the cylinder of
483 RGB LEDs. The assay was enclosed in a black 1/4" thick acrylic box of dimensions 15" x 15" x
484 28" to prevent ambient light from entering the assay. The top of the acrylic box had an entry
485 port of 4" x 2.7" for CO₂ diffused by a Flystuff Flypad (Genesee Scientific, 59-114), and two
486 doors on the side, one at the level of the cylinder (10" high x 8" wide) and one at the bottom (8"
487 high x 10" wide) at the level of the camera. The day before the experiment, mosquitoes were
488 sexed under cold anaesthesia in white light, placed into the cylindrical canisters, and fed water
489 and 400 μ M all-trans retinal in the dark until the experiment commenced. Dental wicks were
490 soaked in approximately 12.5 mL of the water and all-trans retinal, placed on top of the mesh
491 of the inset lid. Trials were run in an environmental room at 25-28°C and 70-80% humidity. For
492 each trial, a canister of 20 mosquitoes was placed on the platform and acclimated for 10
493 minutes prior to the stimulus. Throughout the acclimation period and trial, the canister was
494 bathed in dim blue 471 nm light from the RGB LEDs. At the start of the trial, a blood meal
495 consisting of 5 mL of defibrinated sheep blood (Hemostat Laboratories DSB100) with 2 mM
496 ATP (Sigma A6419-1G) heated to 42°C was placed on top of the canister. Blood meals were
497 delivered using an acrylic lid consisting of a 1/16" thick clear acrylic ring with a 2" inner
498 diameter and 2.6" outer diameter attached to a 1/2" thick clear acrylic ring with a 2.3" inner
499 diameter and 2.6" outer diameter. This lid was covered with Parafilm on the 1/16" thick side to
500 create a well for the blood when placed Parafilm-down on the inset lid of the cylindrical
501 canister. At the start of the experiment, the warm blood meal was pipetted onto the Parafilm.
502 On top of the blood meal was an inverted 4 oz bottle (SKS Bottle & Packaging 0604-07) filled

503 with water heated to 42°C to keep the blood near body temperature for the duration of the 15
504 minutes trial. Mosquitoes were given CO₂, red light (624 nm, 3.5-6 μW/mm²), or neither
505 stimulus throughout the 15-minute trial. 10% CO₂ was mixed with filtered room air using flow
506 controllers (Aalborg P26A1-BA2) to deliver a 2.7% CO₂ stimulus through the top of the
507 container. Air flow delivery is described in detail in (Basrur et al., 2020). Between trials, the
508 lower door was opened for 5 minutes with the air flow on to flush residual CO₂ from the assay.
509 On a given day of experiments, each of 3 genotypes (*Gr3*, *CsChrimson*, and *Gr3 >*
510 *CsChrimson*) was tested with each of the 3 stimuli (no stimulus, CO₂, red light), for a total of 9
511 trials. The order of trials was rotated between days. Genotypes were blinded to the
512 experimenter. Attraction to the warm blood meal was quantified by manually counting the
513 number of mosquitoes on the warm blood meal in the video (1 frame/second) every 15
514 seconds. Engorgement was quantified by visual examination of mosquitoes at 4°C after the
515 end of the trial. Between days of experiments, the canisters were cleaned by spraying 70%
516 ethanol with a spray bottle and wiping down with a soft sponge, rinsed with deionized water,
517 and air dried.

518

519 **Opto-thermocycler assay**

520 The opto-thermocycler assay was constructed on top of a PCR thermocycler (Eppendorf
521 Mastercycler) using optomechanical components (Thorlabs XE25L12, XE25L24, XE25L09,
522 XE25T4, RA90, TRA6, TR12). This assay was used as the basis for experiments delivering
523 light only, light along with heat stimuli, and opto-feeder experiments. Light was delivered using
524 six red light 627nm LEDs (Luxeon Star SP-01-D9) or six green light 530nm LEDs (Luxeon Star
525 SP-01-G4) controlled with an Arduino Uno board. Light intensity was measured using a
526 Coherent Wand UV/VIS Power Sensor (1299161). The surface of the PCR block was covered
527 in black tape to reduce glare (Thorlabs T137-2.0). Temperature was measured using a type T
528 thermocouple (Harold G. Schaevitz Industries LLC CPTC-120-X-N) connected to the Arduino
529 board (Arduino A000066) using a thermocouple amplifier (Adafruit MAX31856). The
530 thermocouple sensor was placed on the surface of the lower right of the PCR block and
531 secured using black tape (Thorlabs T137-2.0). Temperature reading and light output were
532 recorded every 100 milliseconds from the Arduino using a custom Processing script. Video
533 was synchronized with the light and temperature stimuli with an infrared 940 nm LED (Adafruit
534 387) covered with tape and placed in the field of view of the camera. Mosquitoes were
535 illuminated with an infrared 850 nm LED strip (Waveform Lighting 7031.85) surrounding the
536 plate of mosquitoes orthogonal to the view of the camera. Video was recorded using a Blackfly
537 camera (FLIR BFS-U3-16S2M-CS) outfitted with a 780 nm longpass filter (Vision Light Tech
538 LP780-25.5) at 30 frames/second using Spinview software. Heat stimuli were programmed
539 onto the PCR thermocycler to elicit the desired change in temperature from ambient to skin
540 temperature (25-35°C) as measured by the thermocouple (Figure 2B). Red light stimuli were
541 627 nm at an intensity of 12 μW/mm², chosen as the minimum intensity that gave close to the
542 maximum behavioral response. Green light stimuli were 530 nm at an intensity of 22 μW/mm²,
543 chosen because it was the maximum intensity of our setup and to maximize the chance of
544 observing a persistent response to green light. To synchronize the heat and light stimuli,
545 experiments started with a brief dip in temperature followed by a 10-minute acclimation period
546 after which the experiment started. Experiments in Figure 2E-H were conducted with a single
547 stimulus presented to mosquitoes to determine the duration of response. In all other
548 experiments, mosquitoes received multiple stimuli over the course of a 3–6-hour experiment.

549 Data from the rare trials where the mosquito died during the experiment were discarded. For
550 experiments using red light and heat, trials were delivered 20 minutes apart and the order was
551 pseudorandomized between multiple sweeps of trials and across days. For experiments using
552 green light and heat (**Figure 2I,K**), the stimuli were pseudorandomized across sweeps only.
553 Mosquitoes were assayed in a custom acrylic plate with 3 x 5 wells. The sides of the plate
554 were cut using a laser cutter from 1/8" thick clear acrylic, then assembled using acrylic glue
555 (WELD-ON, #4SC Plastic Solvent Glue for Acrylic). The top and bottom were cut from 1/16"
556 acrylic. The top was left removable to load mosquitoes while the bottom was used to sandwich
557 a piece of black fiberglass window screen (Breakthrough Premium Products IHLRS3684BL)
558 creating a mesh bottom for each well. The acrylic bottom piece spaced the mesh bottom of the
559 wells 1.5 mm from the surface of the PCR block. Wells containing the mosquitoes were 18.5
560 mm long x 17 mm wide x 12 mm high. The well in the lower right was empty to accommodate
561 the thermocouple. The day before the experiment, mosquitoes were sexed under cold
562 anesthesia in white light, placed into the custom plate, and fed water and 400 μ M all-trans
563 retinal overnight until the experiment. This was delivered in cotton dental wicks each soaked
564 with 12.5 mL water and all-trans retinal. Three wicks were laid flat beneath each plate so that
565 mosquitoes in all wells could access the wicks beneath. Experiments were run at ambient
566 room temperature and humidity, but the PCR block kept the assay chamber at a fixed
567 temperature. Between trials the surface of the PCR block was cleaned by wiping with a
568 Kimwipe moistened with 70% ethanol. Between days of experiments, the canisters were
569 cleaned by spraying 70% ethanol with a spray bottle and wiping down with a gloved finger,
570 rinsed with deionized water, and air dried.

571 572 **Opto-feeder assay**

573 The opto-thermocycler assay captures probing behavior but does not offer a meal for
574 engorgement. We therefore modified this device to produce the opto-feeder. The most
575 biologically relevant meal for host-seeking females would be blood, but its opacity makes it
576 unsuitable for our video tracking. We therefore used adenosine 5'-triphosphate (ATP) in saline
577 as a an optically clear proxy for blood. This meal has previously been shown to be highly
578 palatable and triggers mosquito engorgement equivalent to a blood meal (**Galun et al., 1963,**
579 **Jové et al., 2020**). To modify the opto-thermocycler to accommodate this blood meal
580 substitute, a thin aluminum plate (McMaster-Carr 6061 Aluminum sheet 0.025") was
581 sandwiched between laser cut pieces of acrylic creating wells on the side facing the mosquito.
582 The wells were 18.5 x 17 x 1 mm. The acrylic was bonded to itself using acrylic glue (WELD-
583 ON, #4SC Plastic Solvent Glue for Acrylic) and to the aluminum plate with epoxy (Loctite
584 1363118) and UV-curing glue (Bondic SK8024). The plate was prepared for a trial by adding
585 500 μ L of the meal (110 mM NaCl, 20 mM NaHCO₃, and 2 mM ATP) to each well of the plate
586 in **Figure 4A-C**. In **Figure 4D-F**, the composition of the meal was 110 mM NaCl, 10 mM
587 NaHCO₃, and 2 mM ATP. The plate was covered with Parafilm to provide a membrane for the
588 mosquitoes to pierce before accessing the meal. The plate was placed directly on top of the
589 PCR bock to allow maximum heat transfer. The thermocouple was placed on the surface of the
590 Parafilm in the middle of the well in the lower right corner to record the temperature of the
591 heated meal. Trials were carried out and synchronized in the same way as opto-thermocycler
592 experiments. All opto-feeder experiments were single trial.

593
594

595 **Machine-learning based behavior classification**

596 Videos were pre-processed using a custom Python script `tracking_optothermo.py` that
597 converted the file format, split up videos into ~30-minute chunks, selected frames to create a
598 background image for centroid tracking, and detected frames where the IR synchronization
599 LED was illuminated. Next, we used Ctrax (**Branson et al., 2009**) for centroid tracking. A
600 background model was created using the selected frames from the experimental video. Ctrax
601 background settings were background brightness high threshold 2.55, low threshold 0.25-0.5
602 adjusted depending on the video. The area with the infrared synchronization LED was
603 excluded using a region of interest to avoid interference with the tracking. Mosquitoes that
604 moved very little, such that they were visible in the background image, were corrected for
605 using the Fix Background Model option. In tracking settings, shapes were filtered using the
606 following minimum/maximum: 110/1600 for area, 4/36 for major axis, 4/30 for minor axis,
607 0.0/0.98 for eccentricity. The rest of the tracking settings were default. We used Ctrax centroid
608 tracking as input to Animal Part Tracker (APT, <https://github.com/kristinbranson/APT>
609 downloaded on July 9, 2020) for tracking points on the mosquito body. For opto-thermocycler
610 experiments we tracked 9 points: the tip and base of the proboscis, the tip of the abdomen,
611 and 3 points on each foreleg: where the femur connects to the body, the joint between the
612 femur and the tibia, and the joint between the tibia and the first tarsomere. Opto-thermocycler
613 classifiers were trained on 320 frames from two videos for female mosquitoes and 102 frames
614 from one video for male mosquitoes. We tracked 13 points for opto-feeder experiments, the
615 same 9 points as for opto-thermocycler experiments plus two points at the point of the
616 abdomen where it connects to the thorax and two points at the midpoint or thickest part of the
617 abdomen. The opto-feeder classifier was trained on 215 frames from four videos. All APT
618 classifiers were trained using the Cascaded Pose Regression tracking algorithm. Janelia
619 Automatic Animal Behavior Annotator [(JAABA) (**Kabra et al., 2013**), downloaded on July 15
620 2020] was used for classifying specific behaviors. The classifier for flight (called fly2) was used
621 for all videos of females and males. It was trained from two videos and used appearance and
622 locomotion features with radius of 10 frames with no post-processing. The other classifiers
623 additionally used APT information, a larger radius of frames, and minimum bout sizes for
624 improved accuracy. Separate classifiers were trained for females and males in the opto-
625 thermocycler and females in the opto-feeder experiments to maximize classifier accuracy in
626 the face of differences in visual appearance. Probing classifiers (probe5 for female opto-
627 thermocycler experiments, probemale for male opto-thermocycler experiments, and probeBB
628 for females in the opto-feeder experiments) included the pair of points proboscis tip and base
629 as features, along with APT, motion, and appearance features. The grooming and walking
630 classifiers (walk3 for female and male opto-thermocycler experiments, groom3 and groommale
631 for female and male opto-thermocycler experiments, respectively, and walkBB and groomBB
632 for opto-feeder experiments) were trained using APT, locomotor, and appearance features.
633 APT classifiers were visually inspected for accuracy. APT and JAABA classifiers were
634 evaluated by the accuracy of ground truthing on the JAABA classifiers. An initial classifier was
635 trained, then ground truthing was performed on 50-100 segments of 1 second video segments
636 that were balanced between segments with and without the behavior. These segments were
637 examined for mis-classified frames and additional training was performed to improve the
638 classifier. Thus, the ground truth dataset is more challenging than a random one because it
639 contains frames that were previously mis-classified and so the real accuracy is higher. Training
640 continued until true positive and true negative rates of were >90% were obtained with 7 of 9

641 classifiers. Two other classifiers had rates slightly below this. The groomBB was trained to
642 ~84% true positive and negative rate because certain grooming postures are difficult to
643 distinguish from probing postures. The probemale classifier was trained to ~87% true positive
644 and ~91% true negative rate because only part of the male proboscis is distinguishable from
645 the maxillary palps during probing behavior. Classified behaviors for each mosquito track from
646 JAABA were assigned to single wells according to x-y location of the track to correct the small
647 numbers of frames where Ctrax detected two mosquitoes per well (usually due to a leg that
648 was discontinuous with the rest of the animal) and to connect broken tracks to a single
649 individual mosquito. The IR LED stimulus in the video was aligned with data about temperature
650 and light stimuli from the Arduino and assigned to frames in the video. Velocity was calculated
651 by taking the Ctrax x-y position at 100 ms intervals (3 frames).

652

653 **Analysis of behavior**

654 To calculate the half-life of the mosquito behavior response in [Figure 2H-J](#) and [Figure 3C,H](#),
655 the baseline was calculated as the average probing in 2 minutes prior to stimulus onset. A
656 sliding window of the amount of probing was calculated in 15 second windows starting at
657 stimulus onset for every frame. The maximum response was defined as the window with the
658 greatest probing after stimulus onset and $t_{1/2}$ was defined as the first window in which the
659 probing was halfway between the maximum response and the baseline. To calculate the
660 integration of heat and the second stimuli (fictive CO₂, fictive sugar, or green light) in [Figure](#)
661 [2—figure supplement 2](#) and [Figure 2M](#), we calculated the average response to each of the
662 individual stimuli. We added the two responses to get a predicted additive response. For each
663 individual mosquito, we divided its response by the predicted additive response and multiplied
664 by 100%. This gave a percent additivity where 0% was no response and 100% was exactly
665 additive. For line graphs, the additivity signal was smoothed over 4.5 seconds around each
666 500-millisecond timepoint.

667

668 **tSNE analysis**

669 To infer the state of individual mosquitoes in the opto-feeder experiment, we split each
670 mosquito track into 30 second intervals at 10 second step size and calculated 38 parameters.
671 The 30 second time interval was selected as a period of time over which the behaviors
672 exhibited were relevant to interpreting the internal state of the mosquito. The time interval was
673 varied from 10 to 60 seconds to assure that the results were not sensitive to this parameter
674 choice ([Figure 4—figure supplement 2](#)). The parameters included the proportion of the time
675 window that mosquitoes exhibited each behavior and no behavior. Mosquitoes can probe and
676 walk at the same time so the proportion of time probing and walking, probing not walking, and
677 walking not probing were included. The number of bouts of each behavior was included.
678 Velocity parameters included average velocity over the window and average velocity during
679 each behavior. Transitions between behaviors were included as outgoing rate per second of
680 transition to all other behaviors or no behavior. For the purposes of transitions and ethograms,
681 probing and walking were treated as mutually exclusive with probing taking higher precedence
682 over walking. For all behaviors to avoid rare frames where multiple behaviors were classified
683 for a single frame the precedence of behaviors were flying > probing > walking > grooming >
684 no behavior. Based on the total amount of time animals spent performing each behavior,
685 cutoffs were determined to specify a minimum amount of behavior exhibited. Cutoffs were 0.04
686 for flight, 0.2 for walking or probing, and 0.3 for grooming. Behavior below these cutoffs was

687 excluded from further analysis. The Python package scikit-learn (<https://scikit-learn.org/>
688 version 0.24.1) was used for tSNE embedding with parameters n/100 perplexity (1061), and
689 other default parameters (200 learning rate, 1000 iterations). Multiple perplexities were
690 compared to assure that results were not sensitive to this parameter choice. tSNE plots were
691 examined and clusters were segmented manually by grouping densely clustered points. These
692 clusters were used to annotate videos for visual inspection of what mosquito behaviors they
693 corresponded to. Names for clusters were chosen based on the characteristics of the clusters
694 shown in [Figure 4K](#), [Figure 4—figure supplement 1B](#), [Figure 4—figure supplement 2](#), and
695 video observation. Clusters that included mosquitoes that moved around were named Global
696 or Local search based on the total amount of movement and contrasting amounts of flight and
697 walk behaviors. The cluster that included mostly grooming was termed Rest. The cluster that
698 included mosquitoes that were stationary, probing, and with abdomens expanded after feeding
699 was termed Engorge. The clusters for Rest, Global Search, and Local Search were single
700 clusters that were clearly differentiated on the tSNE embedding. The Engorge cluster was
701 composed of two smaller clusters that, when observed on video, both consisted of mosquitoes
702 engorging and were therefore combined. Points on the end of the Local Search cluster in the
703 tSNE embedding with high probing were also examined by video and grouping was kept with
704 the Local Search cluster.

705

706 **Statistical analyses**

707 R (<https://www.r-project.org> version 4.0.5) and Python were used for statistical analysis. Data
708 distributions were visually examined for normality or tested using the Shapiro-Wilk test.
709 Normally distributed samples were compared by one sample t-test for paired measurements or
710 ANOVA and Tukey's test for multiple categories. Non-normally distributed samples were
711 compared using the Friedman test for multiple category repeated measurements, Kruskal-
712 Wallis test for multiple category single measurements, or the sign test for skewed paired
713 measurements. The Friedman and Kruskal-Wallis test were used with Nemenyi post-hoc tests
714 to determine pairwise differences between categories. T-tests and sign tests were adjusted
715 using Holm's method for correcting for multiple comparisons. For statistical analyses involving
716 comparisons of the behavior of males and females, we repeated the tests after accounting for
717 differences in classifier accuracy by changing the proportion of behavior by this difference (i.e.
718 4.93% for probing and 3.25% for walking) and confirming that the results were the same.
719 Sample sizes followed conventions in the field. For experiments with multiple stimuli presented
720 to each animal, 4-6 days of data were collected. For endpoint and single stimulus experiments,
721 7-11 days of data were collected.

722

723 **Logistic Regression**

724 Logistic regression models for the opto-feeder experiment were trained using the Python
725 sklearn package with the proportion of time mosquitoes spent in each of the four behaviors
726 (groom, walk, probe, and fly) for two minutes after the light stimulus as predictors. These
727 periods of time were -2 to 0 minutes, -8 to -6 minutes, and -14 to -12 minutes relative to the
728 heat stimulus for the 2-minute, 8-minute, and 14-minute inter stimulus interval experiments.
729 The dependent variable was whether the mosquito engorged by the end of the experiment.
730 Models used the liblinear solver, random_state of 0, and balanced weight_class. Bootstrapping
731 was performed using 10,000 resamples with replacement of the engorgement dataset to
732 determine the distribution of predictive models. 10,000 shuffles of the engorgement data were

733 used to determine whether the predictive model performed above chance. Leave-one-out
734 cross-validation was used to determine whether the model was overfitted.

735

736 **Data availability**

737 Data presented in main and supplementary figures is available in [Supplementary File 1](#). Large
738 datasets are available at <https://github.com/trevorsorrells/Optothermocycler>.

739

740 **Code availability**

741 Analysis code used in this publication is available at
742 <https://github.com/trevorsorrells/Optothermocycler>.

743

744 **References**

- 745 Álvarez-Salvado E, Licata AM, Connor EG, McHugh MK, King BM, Stavropoulos N, Victor JD,
746 Crimaldi JP, Nagel KI. 2018. Elementary sensory-motor transformations underlying olfactory
747 navigation in walking fruit-flies. *Elife* **7**: e37815.
- 748 Anholt BR, Ludwig D, Rasmussen JB. 1987. Optimal pursuit times: How long should predators
749 pursue their prey? *Theor Popul Biol* **31**: 453-464
- 750 Araripe LO, Bezerra JRA, Rivas G, Bruno RV. 2018. Locomotor activity in males of *Aedes*
751 *aegypti* can shift in response to females' presence. *Parasit Vectors* **11**: 254
- 752 Asahina K, Watanabe K, Duistermars BJ, Hoopfer E, Gonzalez CR, Eyjolfsdottir EA, Perona P,
753 Anderson DJ. 2014. Tachykinin-expressing neurons control male-specific aggressive arousal
754 in *Drosophila*. *Cell* **156**: 221-235
- 755 Basrur NS, De Obaldia ME, Morita T, Herre M, von Heynitz RK, Tsitohay YN, Vosshall LB.
756 2020. *Fruitless* mutant male mosquitoes gain attraction to human odor. *Elife* **9**: e63982
- 757 Bertossa RC, van de Zande L, Beukeboom LW. 2009. The *fruitless* gene in *Nasonia* displays
758 complex sex-specific splicing and contains new zinc finger domains. *Mol Biol Evol* **26**: 1557-
759 1569
- 760 Branson K, Robie AA, Bender J, Perona P, Dickinson MH. 2009. High-throughput ethomics in
761 large groups of *Drosophila*. *Nat Methods* **6**: 451-457
- 762 Chari T, Banerjee J, Pachter L. 2021. The specious art of single-cell genomics. *bioRxiv*: DOI
763 10.1101/2021.1108.1125.457696
- 764 Clowney EJ, Iguchi S, Bussell JJ, Scheer E, Ruta V. 2015. Multimodal chemosensory circuits
765 controlling male courtship in *Drosophila*. *Neuron* **87**: 1036-1049
- 766 Corfas RA, Vosshall LB. 2015. The cation channel TRPA1 tunes mosquito thermotaxis to host
767 temperatures. *Elife* **4**: e11750

- 768 DeGennaro M, McBride CS, Seeholzer L, Nakagawa T, Dennis EJ, Goldman C, Jasinskiene
769 N, James AA, Vosshall LB. 2013. *orco* mutant mosquitoes lose strong preference for humans
770 and are not repelled by volatile DEET. *Nature* **498**: 487-491
- 771 Dekker T, Carde RT. 2011. Moment-to-moment flight manoeuvres of the female yellow fever
772 mosquito (*Aedes aegypti* L.) in response to plumes of carbon dioxide and human skin odour. *J*
773 *Exp Biol* **214**: 3480-3494
- 774 Dekker T, Geier M, Carde RT. 2005. Carbon dioxide instantly sensitizes female yellow fever
775 mosquitoes to human skin odours. *J Exp Biol* **208**: 2963-2972
- 776 Demir E, Dickson BJ. 2005. *fruitless* splicing specifies male courtship behavior in *Drosophila*.
777 *Cell* **121**: 785-794
- 778 Demir M, Kadakia N, Anderson HD, Clark DA, Emonet T. 2020. Walking *Drosophila* navigate
779 complex plumes using stochastic decisions biased by the timing of odor encounters. *Elife* **9**:
780 e57524
- 781 Duvall LB, Basrur NS, Molina H, McMeniman CJ, Vosshall LB. 2017. A peptide signaling
782 system that rapidly enforces paternity in the *Aedes aegypti* mosquito. *Curr Biol* **27**: 3734-3742
- 783 Eiras AE, Jepson PC. 1991. Host location by *Aedes aegypti* (Diptera: Culicidae): a wind tunnel
784 study of chemical cues. *B Entomol Res* **81**: 151-160
- 785 Endler JA. 1991. Interactions between predators and prey. In *Behavioral Ecology*, Krebs JR,
786 Davies NB (eds) pp 169-196. Oxford, UK: Blackwell
- 787 Flavell SW, Pokala N, Macosko EZ, Albrecht DR, Larsch J, Bargmann CI. 2013. Serotonin and
788 the neuropeptide PDF initiate and extend opposing behavioral states in *C. elegans*. *Cell* **154**:
789 1023-1035
- 790 Galun R, Avi-Dor Y, Bar-Zeev M. 1963. Feeding response in *Aedes aegypti*: Stimulation by
791 adenosine triphosphate. *Science* **142**: 1674-1675
- 792 Geier M, Bosch OJ, Boeckh J. 1999. Influence of odour plume structure on upwind flight of
793 mosquitoes towards hosts. *J Exp Biol* **202**: 1639-1648
- 794 Grant AJ, O'Connell RJ. 2007. Age-related changes in female mosquito carbon dioxide
795 detection. *J Med Entomol* **44**: 617-623
- 796 Grant AJ, Wigton BE, Aghajanian JG, O'Connell RJ. 1995. Electrophysiological responses of
797 receptor neurons in mosquito maxillary palp sensilla to carbon dioxide. *J Comp Physiol [A]*
798 **177**: 389-396
- 799 Han W, Tellez LA, Rangel MJ, Jr., Motta SC, Zhang X, Perez IO, Canteras NS, Shammah-
800 Lagnado SJ, van den Pol AN, de Araujo IE. 2017. Integrated control of predatory hunting by
801 the central nucleus of the amygdala. *Cell* **168**: 311-324

- 802 Hartberg WK. 1971. Observations on the mating behaviour of *Aedes aegypti* in nature. *Bull*
803 *World Health Organ* **45**: 847–850
- 804 Hindmarsh Sten T, Li R, Otopalik A, Ruta V. 2021. Sexual arousal gates visual processing
805 during *Drosophila* courtship. *Nature* **595**: 549-553
- 806 Inagaki HK, Jung Y, Hoopfer ED, Wong AM, Mishra N, Lin JY, Tsien RY, Anderson DJ. 2014.
807 Optogenetic control of *Drosophila* using a red-shifted channelrhodopsin reveals experience-
808 dependent influences on courtship. *Nat Methods* **11**: 325-332
- 809 Jové V, Gong Z, Hol FJH, Zhao Z, Sorrells TR, Carroll TS, Prakash M, McBride CS, Vosshall
810 LB. 2020. Sensory discrimination of blood and floral nectar by *Aedes aegypti* mosquitoes.
811 *Neuron* **108**: 1163–1180
- 812 Jung Y, Kennedy A, Chiu H, Mohammad F, Claridge-Chang A, Anderson DJ. 2020. Neurons
813 that function within an integrator to promote a persistent behavioral state in *Drosophila*. *Neuron*
814 **105**: 322-333
- 815 Kabra M, Robie AA, Rivera-Alba M, Branson S, Branson K. 2013. JAABA: interactive machine
816 learning for automatic annotation of animal behavior. *Nat Methods* **10**: 64-67
- 817 Klapoetke NC, Murata Y, Kim SS, Pulver SR, Birdsey-Benson A, Cho YK, Morimoto TK,
818 Chuong AS, Carpenter EJ, Tian Z, Wang J, Xie Y, Yan Z, Zhang Y, Chow BY, Surek B,
819 Melkonian M, Jayaraman V, Constantine-Paton M, Wong GK et al. 2014. Independent optical
820 excitation of distinct neural populations. *Nat Methods* **11**: 338-346
- 821 Klowden M. 1981. Initiation and termination of host-seeking inhibition in *Aedes aegypti* during
822 oöcyte maturation. *J Insect Physiol* **27**: 799-803
- 823 Koehl MA. 2006. The fluid mechanics of arthropod sniffing in turbulent odor plumes. *Chem*
824 *Senses* **31**: 93-105
- 825 Körding K. 2007. Decision theory: what "should" the nervous system do? *Science* **318**: 606-
826 610
- 827 Lafferty KD, Kuris AM. 2002. Trophic strategies, animal diversity and body size. *Trends Ecol*
828 *Evol* **17**: 507-513
- 829 Lahondere C, Vinauger C, Okubo RP, Wolff GH, Chan JK, Akbari OS, Riffell JA. 2020. The
830 olfactory basis of orchid pollination by mosquitoes. *Proc Natl Acad Sci U S A* **117**: 708-716
- 831 Manoli DS, Foss M, Villella A, Taylor BJ, Hall JC, Baker BS. 2005. Male-specific *fruitless*
832 specifies the neural substrates of *Drosophila* courtship behaviour. *Nature* **436**: 395-400
- 833 Marques JC, Li M, Schaak D, Robson DN, Li JM. 2020. Internal state dynamics shape
834 brainwide activity and foraging behaviour. *Nature* **577**: 239-243

- 835 Matthews BJ, Dudchenko O, Kingan SB, Koren S, Antoshechkin I, Crawford JE, Glassford WJ,
836 Herre M, Redmond SN, Rose NH, Weedall GD, Wu Y, Batra SS, Brito-Sierra CA, Buckingham
837 SD, Campbell CL, Chan S, Cox E, Evans BR, Fansiri T et al. 2018. Improved reference
838 genome of *Aedes aegypti* informs arbovirus vector control. *Nature* **563**: 501-507
- 839 Matthews BJ, McBride CS, DeGennaro M, Despo O, Vosshall LB. 2016. The
840 neurotranscriptome of the *Aedes aegypti* mosquito. *BMC Genomics* **17**: 32
- 841 McMeniman CJ, Corfas RA, Matthews BJ, Ritchie SA, Vosshall LB. 2014. Multimodal
842 integration of carbon dioxide and other sensory cues drives mosquito attraction to humans.
843 *Cell* **156**: 1060-1071
- 844 Pang R, van Breugel F, Dickinson M, Riffell JA, Fairhall A. 2018. History dependence in insect
845 flight decisions during odor tracking. *PLoS Comput Biol* **14**: e1005969
- 846 Potter CJ, Tasic B, Russler EV, Liang L, Luo L. 2010. The Q system: a repressible binary
847 system for transgene expression, lineage tracing, and mosaic analysis. *Cell* **141**: 536-548
- 848 Riabinina O, Task D, Marr E, Lin CC, Alford R, O'Brochta DA, Potter CJ. 2016. Organization of
849 olfactory centres in the malaria mosquito *Anopheles gambiae*. *Nat Commun* **7**: 13010
- 850 Rudolfs W. 1922. Chemotropism of mosquitoes. *New Jers AES Bull* **367**: 5-23
- 851 San Alberto DA, Rusch C, Zhan Y, Straw AD, Montell C, Riffell JA. 2021. The olfactory gating
852 of visual preferences to human skin and colors in mosquitoes. *bioRxiv*:
853 10.1101/2021.1107.1126.453916
- 854 Stern DL. 2017. Tagmentation-based mapping (TagMap) of mobile DNA genomic insertion
855 sites. *bioRxiv*: DOI: 10.1101/037762
- 856 van Breugel F, Riffell J, Fairhall A, Dickinson MH. 2015. Mosquitoes use vision to associate
857 odor plumes with thermal targets. *Curr Biol* **25**: 2123-2139
- 858 Vergassola M, Villermaux E, Shraiman BI. 2007. 'Infotaxis' as a strategy for searching without
859 gradients. *Nature* **445**: 406-409
- 860 Williams TM, Wolfe L, Davis T, Kendall T, Richter B, Wang Y, Bryce C, Elkaim GH, Wilmers
861 CC. 2014. Mammalian energetics. Instantaneous energetics of puma kills reveal advantage of
862 felid sneak attacks. *Science* **346**: 81-85
- 863 Younger MA, Herre M, Ehrlich AR, Gong ZY, Gilbert ZN, Rahiel S, Matthews BJ, Vosshall LB.
864 2020. Non-canonical odor coding ensures unbreakable mosquito attraction to humans.
865 *bioRxiv*: DOI 2020.2011.2007.368720
866

867 **Acknowledgements**

868 We thank Hessam Akhlaghpour, Josie Clowney, Emily Dennis, Ann Kennedy, Philip Kidd, and
869 members of the Vosshall lab for comments on the manuscript. We thank Allen Lee, Alice
870 Robie, and Kristin Branson for sharing their unpublished Animal Part Tracker and providing
871 technical help with running it. We thank Jason Banfelder and Rebecca Bennett with software
872 setup on the Rockefeller High Performance Computing Cluster; Jim Petrillo, Dan Gross, and
873 Peer Strogies at the Rockefeller Precision Instrumentation Technologies facility for assistance
874 with design and fabrication of behavior assays; Gloria Gordon and Libby Mejia for expert
875 mosquito rearing; Tom Hindmarsh Sten, Veronica Jové, Gaby Maimon, Ben Matthews Chris
876 Potter, Vanessa Ruta, and Nilay Yapici for discussions; Annie Handler, Jazz Weisman, and Ari
877 Zolin for technical advice with optogenetics experiments; Ben Matthews, Meg Younger, and
878 the Aedes Toolkit Group for access to unpublished strains; Cong Li for assisting with an early
879 version of the individual state analysis; and Rob Harrell at the Insect Transformation Facility for
880 embryo injections. Pilot experiments for this study used an optogenetic setup in the lab of
881 Vanessa Ruta. This work was funded by a Jane Coffin Childs postdoctoral Fellowship (T.R.S.),
882 and a Kavli Neural Systems Institute Pilot Grant and Postdoctoral Fellowship (T.R.S.). L.B.V. is
883 an investigator of the Howard Hughes Medical Institute.

884
885 **Author contributions**

886 T.R.S. performed all experiments and analyses in the paper with the exception of **Figure 4I**,
887 which was performed by A.R.-V. The optogenetic mosquito lines were created and tested by
888 T.R.S, and A.P., who also developed the rearing and experimental protocol. T.R.S and L.B.V.
889 conceived the study, created the figures, and wrote the manuscript with input from all authors.

890
891 **Competing interests**

892 The authors declare no competing interests.

893
894 **Materials & Correspondence**

895 Correspondence and materials requests should be addressed to Trevor Sorrells and Leslie
896 Vosshall.

897
898 **Supplementary figures and tables**

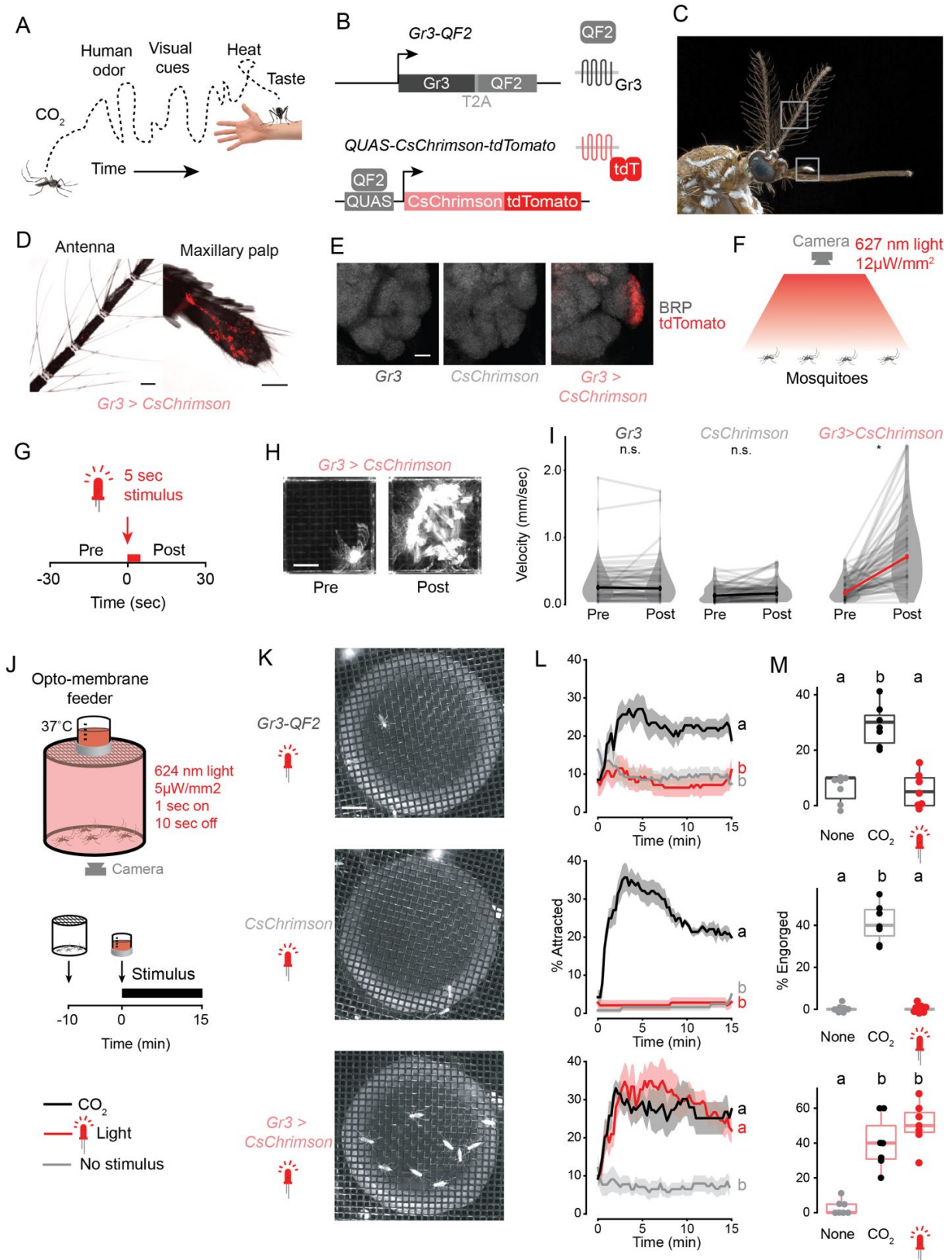
899 **Figure 2—figure supplements 1 and 2**, **Figure 4—figure supplements 1 and 2**, and
900 **Supplementary Video 1** accompany the paper.

901
902 **Supplementary information**

903 **Supplementary File 1** includes information on the accuracy of the behavioral classifier and all
904 raw data and statistical analysis in the paper, including sample sizes, exact p-values, and tests
905 performed.

906
907

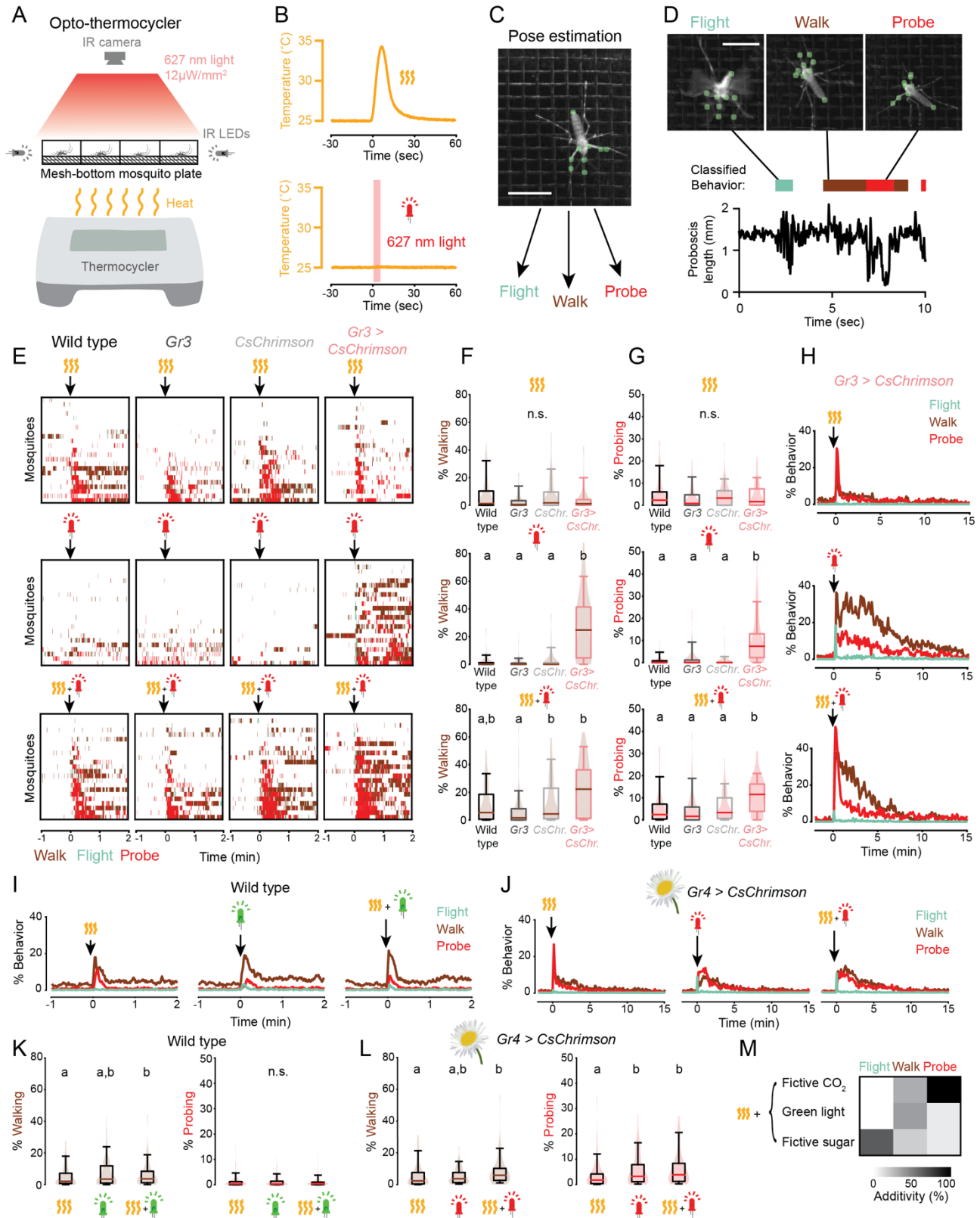
Figure 1



909 **Figure 1.** Optogenetic control of mosquito host seeking and blood feeding. **(A)** Schematic of
910 human host cues experienced by a host-seeking mosquito over time. **(B)** Schematic of genetic
911 reagents used for optogenetic activation of CO₂-sensitive *Gr3* sensory neurons. **(C)** Female
912 *Aedes aegypti*, grey boxes indicating antenna (top) and maxillary palp (bottom). Photo: Alex
913 Wild. **(D)** Intrinsic tdTomato fluorescence of whole mounted *Gr3 > CsChrimson* female
914 mosquito antenna and maxillary palp. Scale bar: 50 μm. **(E)** Maximum-intensity projections of
915 confocal Z-stacks of antennal lobes in the right-brain hemisphere of the indicated genotype
916 with immunofluorescent labelling of tdTomato (red) and the synaptic marker BRP (grayscale).
917 Scale bar: 10 μm. **(F,G)** Diagram **F** and stimulus protocol **G** of optogenetic behavior assay for
918 mosquito movement. **(H)** Time maximum projection of a single mosquito in the assay in **F** for
919 30 seconds pre- (left) and post- (right) stimulus. Scale bar: 0.5 cm. **(I)** Velocity of individual
920 mosquitoes of the indicated genotypes 30 seconds pre- and post-stimulus onset. Data are
921 plotted as mean of individual mosquitoes (thin grey lines) with median across individuals
922 indicated with thick black or red line (**P* < 0.0001, Wilcoxon signed rank test with Holm's
923 correction for multiple comparison, n.s., not significant, n=70 mosquitoes/genotype). **(J)**
924 Schematic of opto-membrane feeder (top) and stimulus protocol (bottom). **(K)** Still images of
925 mosquitoes of the indicated genotype underneath the warm blood meal approximately 7
926 minutes after the start of red-light stimulation. Scale bar: 1 cm. **(L)** Occupancy of mosquitoes
927 on warm blood meal in the opto-membrane feeder. Data are plotted as mean (line) ± S.E.M.
928 (shading). Data labelled with different letters are significantly different at the 5 minute timepoint
929 (*P* < 0.05, Kruskal-Wallis test followed by Nemenyi post-hoc tests; n=6-7 trials per
930 genotype/stimulus combination, 18-21 mosquitoes/trial). **(M)** Percent of mosquitoes visually
931 scored as engorged at the conclusion of the experiment in **L**. Data are plotted as dot-box plots
932 (median: horizontal line, interquartile range: box, 1.5 times interquartile range: whiskers. Data
933 labelled with different letters are significantly different (*P* < 0.05, Kruskal-Wallis test followed by
934 Nemenyi post-hoc tests; n=7 trials per genotype/stimulus combination and 18-21
935 mosquitoes/trial).

936
937

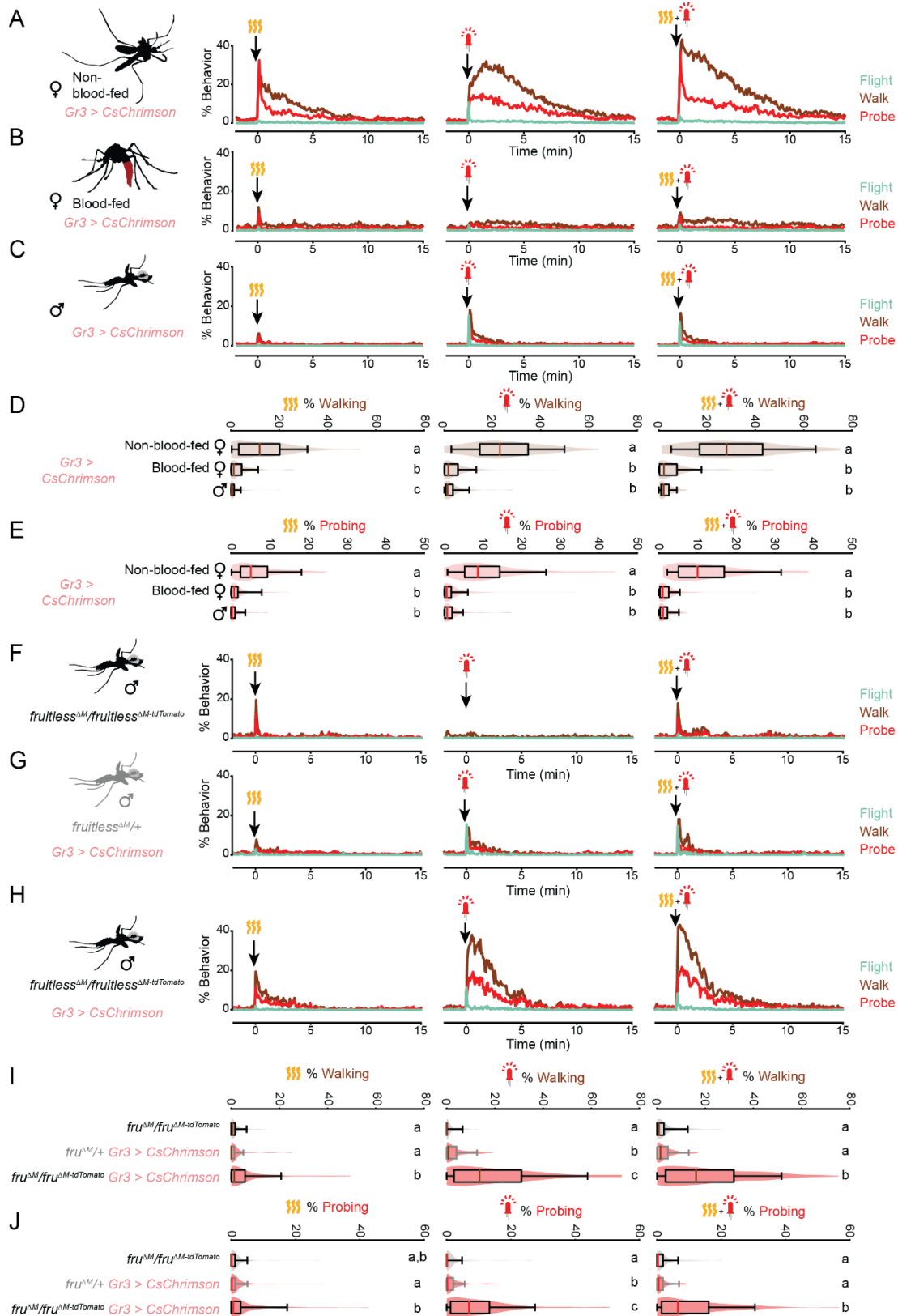
Figure 2



939 **Figure 2.** Fictive CO₂ induces a persistent behavior state. **(A,B)** Schematic of opto-
940 thermocycler assay **A** and stimuli delivered **B**. **(C)** Still image of a mosquito with pose tracking
941 of 9 points using Animal Part Tracker. Scale bar: 0.5 cm. **(D)** Still images of a mosquito
942 exhibiting the indicated classified behaviors (top). Representative plot of proboscis length with
943 classified behavior superimposed (bottom). Scale bar: 0.5 cm. **(E)** Ethograms of individual
944 mosquitoes of the indicated genotypes. Data show 1 minute before and an excerpt of the 2
945 minute after the indicated stimuli from a 20 minute experiment. Each row represents data from
946 one mosquito. The experiment comprised a total of n=68-70 mosquitoes/condition. All data
947 were sorted by probing, and every third mosquito (n=22-23) was selected for display here for
948 clarity. **(F,G)** Quantification of walking **F** and probing **G** behavior exhibited by individual
949 mosquitoes from the experiment in **E** during the 5 minute after stimulus onset. Data are plotted
950 as violin-box plots (median: horizontal line, interquartile range: box, 5th and 95th percentiles
951 indicated: whiskers). Data labelled with different letters are significantly different ($P < 0.05$,
952 Kruskal-Wallis test followed by Nemenyi post-hoc tests, n.s., not significant, n=68-70
953 mosquitoes/genotype, 1 stimulus per trial). **(H)** Plot of percent individual *Gr3 > CsChrimson*
954 mosquitoes exhibiting the indicated behavior from 2 minute before to 15 minutes after stimulus
955 onset. Data from experiment in **E**. **(I,J)** Plot of percent individual wild type **I** and *Gr4 >*
956 *CsChrimson* **J** mosquitoes exhibiting the indicated behavior from 1 minute before to 2 minutes
957 after stimulus onset **I** or 2 minutes before to 15 minutes after stimulus onset **J** excerpted from a
958 20 minute experiment. (**I**: n=140 mosquitoes, average of 2 stimulus presentations/mosquito; **J**:
959 n=69 mosquitoes, average of 3 stimulus presentations/mosquito). Flower image used for *Gr4 >*
960 *CsChrimson* indicates that plant nectar is a sugar source. **(K,L)** Quantification of **I** and **J** for 5
961 minutes after stimulus onset. Data are plotted as violin-box plots (median: horizontal line,
962 interquartile range: box, 5th and 95th percentiles: whiskers). Distribution represents individual
963 mosquitoes, averaged over multiple stimulus presentations. Data labelled with different letters
964 are significantly different ($P < 0.05$, Friedman test followed by Nemenyi post-hoc tests, n.s., not
965 significant). **(M)** Median additivity of heat and the indicated stimuli presented simultaneously.
966 Additivity of 100% corresponds to the) case when combined stimuli equal the sum of
967 responses to individual stimuli. Data from **E-L**. See also [Figure 2—figure supplement 1](#) and
968 [Figure 2—figure supplement 2](#).

969
970

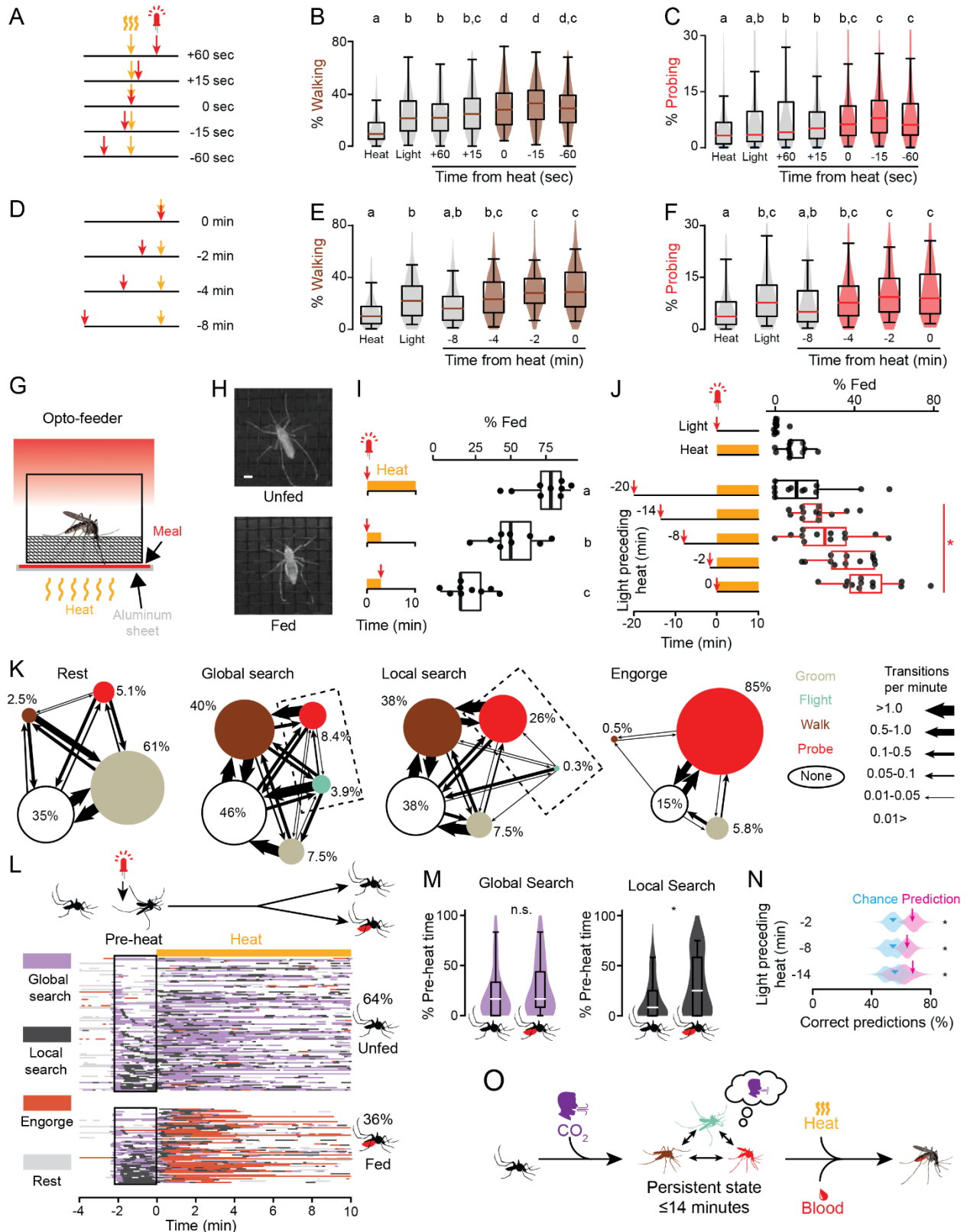
Figure 3



972 **Figure 3.** The persistent state is specific to host seeking. **(A-C)** Response of non-blood-fed
973 female **A**, blood-fed female **B**, and male **C** *Gr3 > CsChrimson* mosquitoes to the indicated
974 stimuli, plotting each behavior from 2 minutes before to 15 minutes after stimulus onset
975 (n=98/group, average of 3 stimulus presentations/mosquito). **(D,E)** Quantification of walking **D**
976 and probing **E** from data in **A-C** for 5 minutes after stimulus onset. **(F-H)** The behavioral
977 response of males of the indicated genotype for 15 minutes after the indicated stimuli, plotting
978 each behavior from 2 minutes before to 15 minutes after stimulus onset (n=97-98/genotype,
979 average of 3 stimulus presentations/mosquito). **(I,J)** Quantification of walking **I** and probing **J**
980 from data in **F-H** for 5 minutes after stimulus onset. In **D,E** and **I,J**, data are plotted as violin-
981 box plots (median: horizontal line, interquartile range: box, 5th and 95th percentiles: whiskers).
982 The distribution represents individual mosquitoes, averaged over multiple stimulus
983 presentations. Data labelled with different letters are significantly different ($P < 0.05$, Kruskal-
984 Wallis test followed by Nemenyi post-hoc tests, n.s., not significant).

985
986

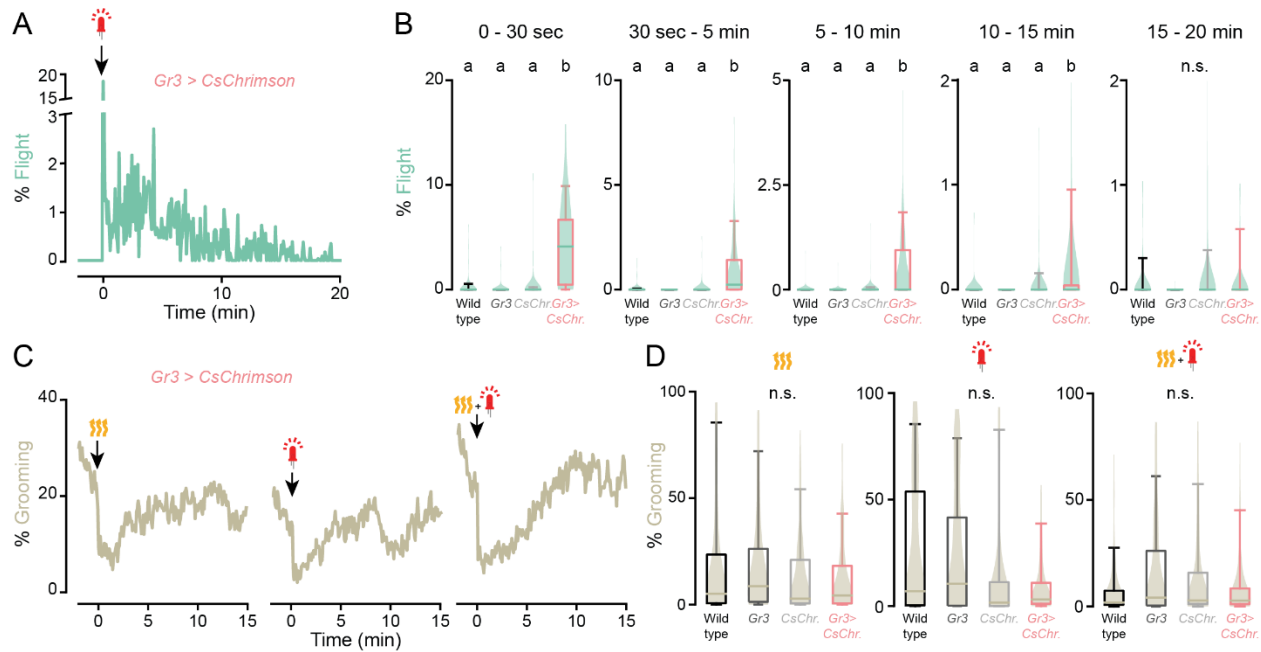
Figure 4



988 **Figure 4.** The persistent state integrates host cues and decision making in time. **(A-F)**
989 Schematic of stimuli presentation **A,D** and quantification of walking **B,E** and probing **C,E** in the
990 5 minutes after the first stimulus onset (n=111-112 mosquitoes, 2 stimulus
991 presentations/mosquito). In **B, C, E,** and **F,** data are displayed as violin-box plots (median:
992 horizontal line, interquartile range: box, 5th and 95th percentiles: whiskers). Data labelled with
993 different letters are significantly different ($P<0.05$, Friedman test followed by Nemenyi post-hoc
994 tests). Data that are significantly different from heat or light are shaded in brown **B,E** or red
995 **C,F.** **(G)** Schematic of opto-feeder assay. **(H)** Still images of unfed (top) and fed (bottom)
996 mosquitoes. Scale bar: 1 mm. **(I)** Percent mosquitoes engorged in response to the indicated
997 stimuli in the opto-feeder assay (n=9 trials/stimulus, 14 mosquitoes/trial). Data labelled with
998 different letters are significantly different ($P<0.05$, ANOVA followed by Tukey's post-hoc test).
999 **(J)** Percent mosquitoes engorged in response to the indicated cues in the opto-feeder assay
1000 (14 mosquitoes/trial n=11 trials/stimulus). Data in **I,J** are displayed as dot-box plots (median:
1001 horizontal line, interquartile range: box, 1.5 times interquartile range: whiskers). Dot-box plots
1002 in **J** with a red border signify data where combined light and heat stimuli are greater than the
1003 sum of individual stimuli ($*P<0.05$, Student's t-test, after adjustment for multiple comparisons
1004 using Holm's method). **(K)** Transition ethograms for each of the four states indicating the
1005 proportion of each behavior and the rate of transitions between them, with dashed rectangle
1006 highlighting difference between global and local search. See also [Figure 4—figure supplement 1](#)
1007 and [Figure 4—figure supplement 2](#). **(L)** Inferred states of 168 individual mosquitoes from the
1008 2 minutes pre-heat stimulus from experiment in **J,** separated into those that were visually
1009 scored as unfed (top, n=108) or fed (bottom, n=60) at the end of the experiment. Each row
1010 represents data from one mosquito and data are sorted according to the amount of local
1011 search during the pre-heat period. White indicates none of the four states were inferred (i.e.
1012 the mosquito was primarily motionless). **(M)** Quantification of the percent of time mosquitoes
1013 spent in the indicated state during the 2 minutes pre-heat period. Data are plotted as violin-box
1014 plots (median: horizontal line, interquartile range: box, 5th and 95th percentiles: whiskers ($*P<$
1015 0.01 , Mann-Whitney U-test, n.s., not significant). **(N)** Performance of a classifier trained on the
1016 proportion of each behavior in pre-heat period and used to predict feeding (magenta arrow)
1017 along with 10,000 bootstrapped classifiers (magenta violin plot). Chance value (cyan
1018 arrowhead) indicates the median performance of model on 10,000 shuffles (cyan violin plot) of
1019 the feeding data in **J.** (n=166-168 mosquitoes/stimulus, $P=2e-4$, 0.0246, 0.0123 for 2, 8, and
1020 14 minutes pre-heat periods, respectively, bootstrapped z-test). **(O)** Summary of the persistent
1021 internal state for host-seeking behavior. Color of the mosquito silhouettes indicates the
1022 behavior depicted using the colors in **K.**

1023
1024

Figure 2—figure supplement 1



1026

Figure 2—figure supplement 1. Fictive CO₂ triggers flight events for 15 minutes. **(A,C)**

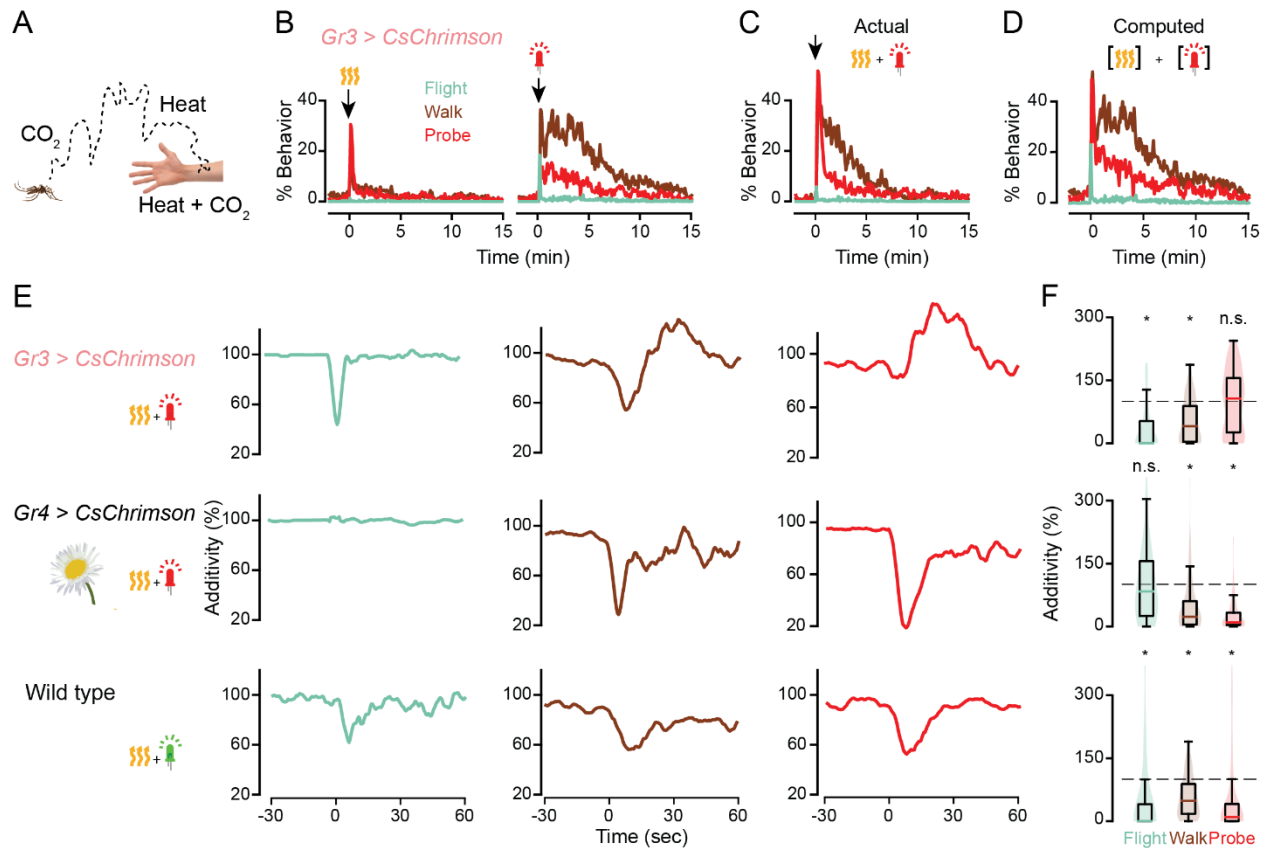
Percent indicated behavior of *Gr3 > CsChrimson* females from 2 minutes before to 15 minutes after stimulus onset in response to the indicated stimuli. Data from **Figure 2E-H**. **(B,D)**

Quantification of the behavior in **A**, **C** along with data collected from the additional indicated genotypes. Data from **Figure 2E-H**. Data are plotted as violin-box plots (median: horizontal line, interquartile range: box, 5th and 95th percentiles: whiskers). Data labelled with different letters are significantly different ($P < 0.05$, Kruskal-Wallis test followed by Nemenyi post-hoc tests. n.s., not significant, $n = 68-70$ mosquitoes).

1034

1035
1036

Figure 2—figure supplement 2



1038

1039

1040

1041

1042

1043

1044

1045

1046

1047

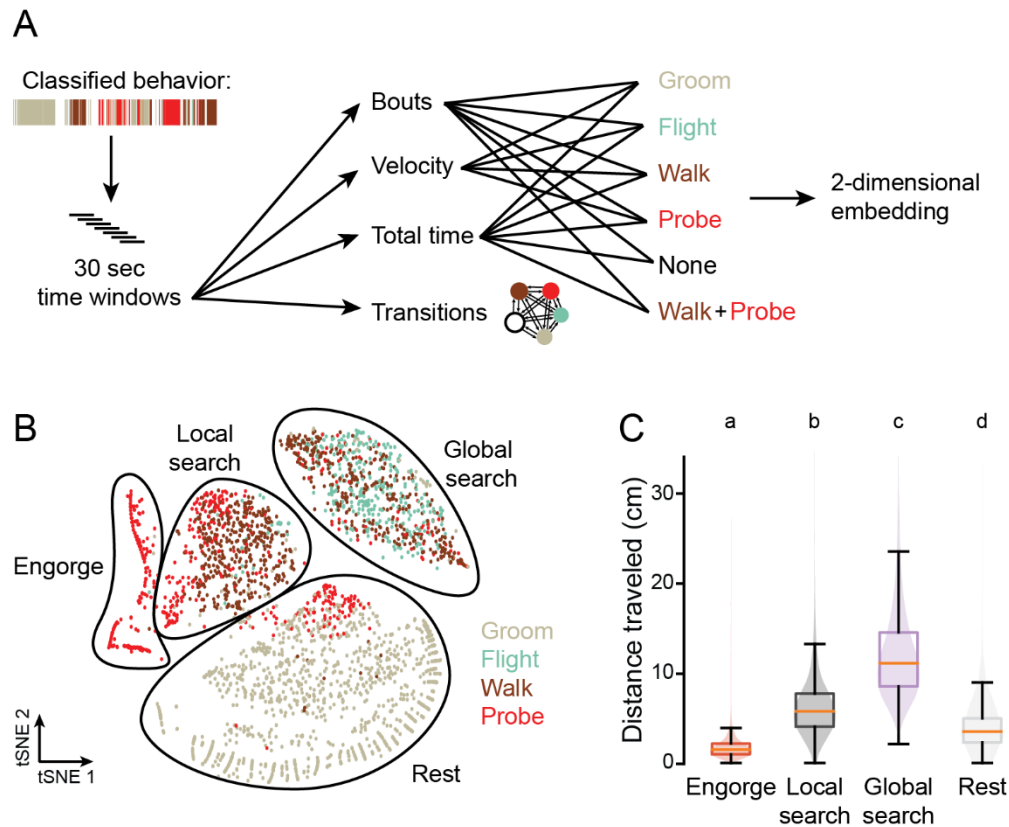
1048

1049

Figure 2—figure supplement 2. Host cues are integrated with different computations than non-host cues. **(A)** Mosquitoes sense host cues separately and simultaneously at different distances from the host. **(B-D)** Responses to individual **B** or combined **C** stimuli or a computed sum of individual stimuli **D**. Plots in **B,C** are reprinted from [Figure 2H](#) for comparison with **D**. **(E)** Differences between calculated and actual responses for the indicated genotypes and stimuli from 30 seconds before to 1 minute after stimulus onset, smoothed using a box filter of radius 2.25 seconds. $n=70$ for *Gr3 > CsChrimson*, $n=69$ for *Gr4 > CsChrimson*, $n=140$ for wild type. **(F)** Quantification of E for the first 15 seconds after stimulus onset. Data are plotted as violin-box plots (median: horizontal line, interquartile range: box, 5th and 95th percentiles: whiskers). (* $P < 0.0001$, sign test using Holm's correction for multiple comparisons, n.s., not significant).

1050
1051

Figure 4—figure supplement 1

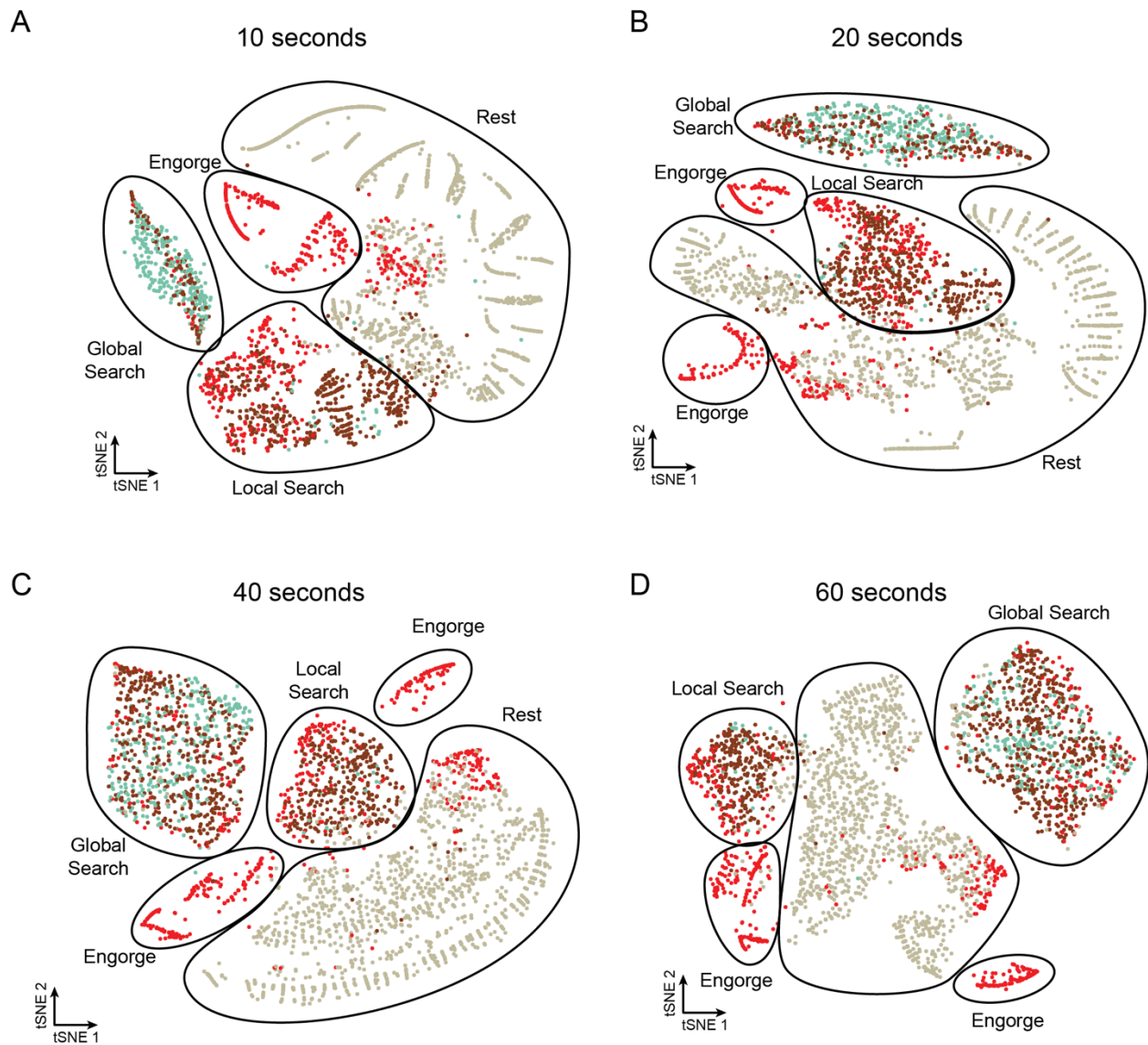


1053
1054
1055
1056
1057
1058
1059
1060
1061
1062
1063
1064
1065
1066
1067
1068
1069

Figure 4—figure supplement 1. Inference of internal state from behavior. **(A)** Schematic of analysis. Classified behavior reflects the output of APT followed by JAABA behavior classifiers. **(B)** t-stochastic neighbor embedding (tSNE) for 30 second time windows spanning 4 minutes prior to the light stimulus to 10 minutes after heat onset for individual mosquitoes from [Figure 4J](#). Points are colored by strong enrichment of the corresponding behavior. State categories were bounded with a black line by visual inspection of the tSNE plot, graphing the behavior characteristics of each cluster, and comparing with video of the mosquitoes in each state. Shown is a random subset of 3,000 time windows from 106,076 total windows from all 7 stimulus types, $n=1,162$ mosquitoes. **(C)** Total distance travelled over the course of 30 second time windows for each behavior state with the following number windows from each state: engorge, $n=5,634$; local search, $n=11,124$; global search, $n=15,466$; rest, $n=9,891$. Time windows were taken from 4 minutes before the light stimulus to 10 minutes after heat onset. Data are plotted as violin-box plots (median: horizontal line, interquartile range: box, 5th and 95th percentiles: whiskers). Data labelled with different letters are significantly different ($P < 0.0001$, Kruskal-Wallis test followed by Nemenyi post-hoc tests).

1070
1071

Figure 4—figure supplement 2



1073
1074
1075
1076
1077
1078
1079

Figure 4—figure supplement 2. Mosquito states are consistent across window duration. (A-D) tSNE for time windows of the indicated duration for individual mosquitoes from Figure 4J. Points are colored by strong enrichment of the corresponding behavior. State categories were bounded with a black line by visual inspection of the tSNE plot. Shown is a random subset of 3,000 time windows from 103,658 A, 105,387 B, 106,044 C, and 105,287 D total windows from all 7 stimulus types, n=1,162 mosquitoes.